Chapter 4

Application examples

This chapter considers applications of the developed theory. Laboratory scale coupled tank and Twin Rotor MIMO system are considered for validation of some of the theoretical results in experimental setups. A boost converter widely used in power electronics applications, is also considered to be an application problem. These applications are highly nonlinear in nature. To cater to nonlinearities involved in their dynamics, and designing controllers using linear control theory is challenging.

Conventionally, there are two approaches for adopting linear control design methods for a nonlinear system. The first one is to linearize the model around an operating point, neglecting the higher order dynamics. This could result in drastic changes in the transient behavior of the model for which the controller fails to ensure robustness and a good tracking response. The second approach is to consider the exact model and represent the nonlinear terms involved, in the form of structural or model uncertainties. The design technique adopted in this chapter is based on the second approach. The nonlinear model of the systems is represented in the form of a polytopic system that allows for the implementation of a linear controller. The variation in nonlinear term is treated as an uncertain parameter for the system representation. A $\mathcal{L}_2$ based Proportional Integral (PI) controller is designed combined with pole placement in a desired LMI region to ensure better transient behavior of the system. Experimental results have been provided and compared with conventional design to illustrate the efficacy of the proposed design method.

Next, this chapter also considers the design of a quasi-Linear Parameter Varying (qLPV) PI controller for Twin Rotor MIMO Systems (TRMS). The nonlinear model is

represented as a qLPV polytopic plant with an affine dependence on a nonlinear parametric function of the pitch angle. This representation retains the exact model as opposed to the conventional linearization around an operating point. Due to the availability of the pitch angle measurement, the nonlinear parameter can be obtained in real-time and the controller is designed using qLPV technique. To deal with limited control input for such systems, the proposed controller design also considers the actuator saturation that yields controller with practical gains without any additional gain bound criterion. Further, the transient tracking performance is also considered in the design by using closed-loop eigenvalues assignment in desired damping regions. The control synthesis problem is formulated in the form of Linear Matrix Inequalities for $\mathcal{L}_2$ gain based performance criterion. The designed controller is validated on a 2-DOF helicopter experimental setup. Finally, to demonstrate the effectiveness of the proposed design, a comparative analysis is done with the existing algorithms. Also, the efficacy of the decentralized controller vis-a-vis the centralized one is presented.

The SOF design criteria presented for polytopic systems subject to actuator saturation in chapter 2 is implemented on the real-time setup of 2-DOF helicopter and experimental results are provided to demonstrate its effectiveness.

For the DT design, we consider the pole-placement criteria in constant damping region, proposed in chapter 3 and implement it on a power electronic boost converter. The objective is to improve its transient behavior subject to variation in input voltage and load resistance. Simulation results are provided to validate the results.

4.1 Continuous-time designs

4.1.1 Coupled Tank System

Proportional-Integral-Derivative (PID) controller, along with many of its other permutations is one of the most ubiquitous linear controllers used in process industry. It has served as one of the main components of numerous distributed and process control systems. Many approaches exist for tuning the P, I and D gains such as root locus, Bode plots, Ziegler-Nichols methods, etc. Unfortunately, a single tuning method usually does not satisfy variety of issues such as load disturbances, measurement noise and model accuracy, though there exist a spectrum of tools that give different types of performances [72].

With the growing need for improved process control, we need to design the controllers in a robust way to extract satisfactory performance even in uncertain environments. A good robust controller should ensure closed-loop system stability and performance over the entire uncertainty domain [62, 74].

Coupled tank system is an example of typical process control system that is widely used in industries such as iron and steel, chemical, petroleum, food processing and pharmaceutical industries, to name a few. The main target at hand is to maintain the desired value of water level in one or both of the tanks. Since the system is governed by a highly nonlinear dynamics, it requires linearization for analysis.

We here propose a new approach to handle the nonlinear dynamics while considering the exact system model. The nonlinear terms have been considered as structural uncertainties, which can be easily represented in the form a polytopic model. Polytopes are the convex representations of uncertain matrices with bounded parameter variations that govern the uncertain system dynamics [3]. These representations are numerically tractable using LMIs [155]. In addition to obtaining a good tracking response, the pole placement method [11,145] is also included in controller design to improve the closed-loop transient behavior that ensures a maximum undamped natural frequency (ω_d), a minimum damping ratio (ζ) and a minimum decay rate (α). This separately bounds various time domain parameters such as delay time, maximum overshoot, settling time and the rise time [12].

The nonlinear dynamics of a coupled tank liquid level system is represented in a linear polytopic form not involving any approximation of the higher order terms. A robust state feedback PI controller is then designed based on LMIs. By placing the closed-loop poles in a desired LMI region, the transient response is satisfactorily improved, thereby ensuring a minimum α and ζ. The designed controller is tested on the system [167] in real time. A comparative performance analyses of proposed design with the conventional PI controller is also done.

4.1.1.1 Mathematical modeling

Fig. 4.1 shows the schematic diagram of the coupled tank system [168] which consists of two cylindrical tanks. V_p denotes the process input voltage to the pump and the output h_1 is the water level of tank 1 and h_2 denotes the water level of tank 2. Our objective

is to control the water level of both the tanks using the pump which feeds input to the upper tank. The nonlinear model can be obtained using the mass balance principle and Bernoulli's law. It is given as

$$\frac{dh_1}{dt} = -\frac{a_{o1}\sqrt{2gh_1}}{a_{t1}} + \frac{K_p V_p}{a_{t1}} \tag{4.1}$$

$$\frac{dh_2}{dt} = \frac{a_{o1}\sqrt{2gh_1}}{a_{t2}} - \frac{a_{o2}\sqrt{2gh_2}}{a_{t2}}. \tag{4.2}$$

where the parameters have been defined in Table 4.1 [167].

Table 4.1: Design parameters for coupled tank system

Parameter	**Definition**	**Value**
K_p	Pump Flow Constant	3.3 $cm^3/s/V$
d_{t1}	Tank 1 inner diameter	4.445 cm
d_{t2}	Tank 2 Inner diameter	4.445 cm
V_{pmax}	Pump Maximum Continuous Voltage	12 V
V_{ppeak}	Pump Peak Voltage	22 V
d_{o1}	Small Outflow Orifice Diameter of tank 1	0.31750 cm
d_{o2}	Small Outflow Orifice Diameter of tank 2	0.31750 cm
h_{1max}	Water Level Range of Tank 1	30 cm
h_{2max}	Water Level Range of Tank 2	30 cm
g	Acceleration due to gravity	981 cm/s^2
K_{L1}	Tank 1 Level Sensor Sensitivity	6.1 cm/V
K_{L2}	Tank 2 Level Sensor Sensitivity	6.1 cm/V

4.1.1.2 Polytopic modeling

This section includes representation of the nonlinear model (4.1) in the form of a polytopic system. Note that, conventional linearization method around the equilibrium point of the nonlinear model is not used for the purpose and hence, the model is free from approximations.

We consider levels h_1 and h_2 as uncertain but bounded, i.e., $h_1 \in [\underline{h}_1, \bar{h}_1]$ and $h_2 \in [\underline{h}_2, \bar{h}_2]$ such that the nonlinearity due to the terms $\rho_1 = \sqrt{\frac{2g}{h_1}}, \rho_1 \in [\underline{\rho}_1, \bar{\rho}_1]$ and $\rho_2 = \sqrt{\frac{2g}{h_2}}, \rho_2 \in [\underline{\rho}_2, \bar{\rho}_2]$ are the uncertain parameters. Here, we have assumed that all

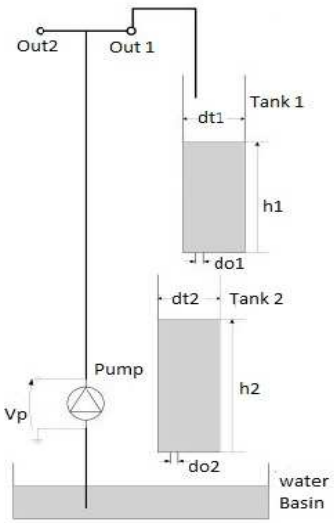

Figure 4.1: Schematic Diagram of Coupled Tank System

the parameters are well known. Thus, in order to counteract changes in the uncertain parameters ρ_1 and ρ_2, we represent the system matrix as a function of these parameters. The nonlinear model (4.1) can be expressed as a linear polytopic one:

$$\begin{aligned} \dot{x}(t) &= A(\rho)x(t) + Bu(t) + B_w w(t), \\ z(t) &= C_z x(t),\ y(t) = Cx(t) \end{aligned} \tag{4.3}$$

where $\rho = [\rho_1 \quad \rho_2]^T$, $x(t) \in \mathbb{R}^2$, $u(t) \in \mathbb{R}^1$ represents the state and control input vector, respectively. $z(t) \in \mathbb{R}^1$ is the controlled output of the system. $w(t) \in \mathbb{R}^1$ and $y(t) \in \mathbb{R}^1$ are exogenous input and measured output, respectively. Here, we have considered only $A(\rho)$ as the parameter dependent matrix. $A(\rho)$, B, B_w and C_z matrices are given by

$$A(\rho) = \begin{bmatrix} -a_{11}\rho_1 & 0 \\ a_{21}\rho_1 & -a_{22}\rho_2 \end{bmatrix}, B = \begin{bmatrix} \eta \\ 0 \end{bmatrix}, B_w = B, C_z = I,$$

where

$$a_{11} = \frac{a_{o1}}{a_{t1}},\ a_{21} = \frac{a_{o1}}{a_{t2}},\ a_{22} = \frac{a_{o2}}{a_{t2}},\ \eta = \frac{K_p}{a_{t1}}.$$

Assumption 2 *For the above system, the following assumptions are taken*

1. *The continuous and bounded system matrix $A(\rho)$ depends affinely on ρ.*

2. ρ varies in a parameter space, which can be represented as a polytope $\mathcal{V}$ as:

$$\rho \in \mathcal{V} := Co\{\nu_1, \nu_2, \nu_3, \nu_4\} = \left\{ \sum_{i=1}^{4} \zeta_i \nu_i : \zeta_i \geq 0, \sum_{i=1}^{4} \zeta_i = 1 \right\}. \tag{4.4}$$

Note that as the number of polytopes increase, the model can definitely incorporate larger uncertainty within itself which results in higher accuracy, but it increases in computational burden as well. Here, only matrix A is a function of the uncertain parameter ρ, and can be expressed as

$$A(\rho) \in \ Co\{A_1, A_2, A_3, A_4\} =: \ \left\{ \sum_{i=1}^{4} \zeta_i A_i, \ \zeta_i \geq 0, \ \sum_{i=1}^{4} \zeta_i = 1 \right\}. \tag{4.5}$$

Considering the Assumption 6, system (4.3) can be represented in polytopic form as:

$$\begin{bmatrix} A(\rho) & B & B_w \\ C_z & 0 & 0 \\ I & 0 & 0 \end{bmatrix} = \sum_{i=1}^{4} \zeta_i(t) \begin{bmatrix} A(\nu_i) & B & B_w \\ C_z & 0 & 0 \\ I & 0 & 0 \end{bmatrix} \tag{4.6}$$

4.1.1.3 Robust $\mathcal{L}_2$ based PI state feedback controller design

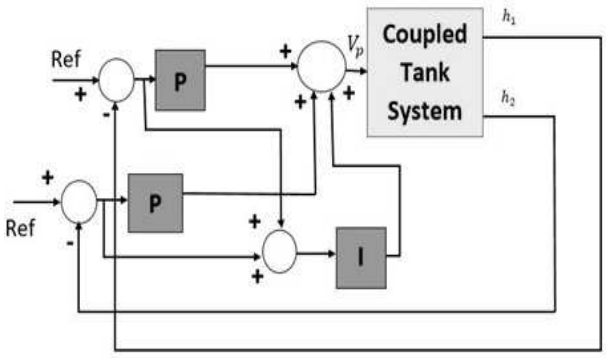

Figure 4.2: Block Diagram of the closed-loop system

Fig. 4.2 shows the closed-loop block diagram of the coupled tank model. The main aim is to design a robust state feedback PI controller for setpoint tracking of water level in the tanks. All the system states $x(t)$ are assumed to be measurable at the output, i.e., $C = I$, and the state information is not corrupted by the input $w(t)$.

4.1.1.4 PI controller design

Let us consider the LTI system (4.3) with PI controller in the form as $u(t) = K_p x(t) + K_I \int_0^t y_t(\tau) d\tau$, $y_t(t) = C_a x(t)$, where $C_a = \begin{bmatrix} 1 & 1 \end{bmatrix}$ involves h_1 and h_2, which are to be

tracked. $K_p \in \mathbb{R}^{2\times 4}, K_I \in \mathbb{R}^{2\times 2}$ are the gain matrices of the PI controller which are to be designed. To design the controller, consider the augmented states [35] as $\tilde{x}(t) = \begin{bmatrix} x^T(t) & \int_0^t y_t^T(\tau)d\tau \end{bmatrix}^T$ with its dynamics as

$$\dot{\tilde{x}}(t) = \bar{A}(\rho)\tilde{x}(t) + \bar{B}u(t) + \bar{B}_w w(t),\ z(t) = \bar{C}_z\tilde{x}(t), \tag{4.7}$$

where $\bar{A}(\rho)$, $\bar{B}$, $\bar{B}_w$ and $\bar{C}_z$ represent the augmented system matrices, given by $\bar{A}(\rho) = \begin{bmatrix} A(\rho) & 0 \\ C_a & 0 \end{bmatrix}$, $\bar{B} = \begin{bmatrix} B \\ 0 \end{bmatrix}$, $\bar{B}_w = \begin{bmatrix} B_w \\ 0 \end{bmatrix}$ and $\bar{C}_z = \begin{bmatrix} C_z & 0 \end{bmatrix}$. For system (4.7), the feedback controller is $u(t) = K\tilde{x}(t)$, where $K = \begin{bmatrix} K_p & K_I \end{bmatrix}$ denotes the controller gain. The closed-loop system is given as:

$$\begin{bmatrix} \dot{\tilde{x}}(t) \\ z(t) \end{bmatrix} = \begin{bmatrix} \bar{A}_{cl}(\rho) & \bar{B}_{cl} \\ \bar{C}_{cl} & 0 \end{bmatrix} \begin{bmatrix} \tilde{x}(t) \\ w(t) \end{bmatrix}, \tag{4.8}$$

where $\bar{A}_{cl}(\rho) = \bar{A}(\rho) + \bar{B}K$, $\bar{B}_{cl} = \bar{B}_w$ and $\bar{C}_{cl} = \bar{C}_z$.

4.1.1.5 $\mathcal{L}_2$ performance criteria

For designing a robust state feedback controller for the system (4.7) with $\mathcal{L}_2$ performance, the below Lemma is well known.

Lemma 4.1 *[3, page 110] There exists a state feedback gain matrix K such that the $\mathcal{L}_2$ gain of the system from input $w(t)$ and output $z(t)$ is less than γ, if there exist matrices $X > 0$ and Z that satisfy the following LMI:*

$$\begin{bmatrix} \bar{A}_i X + X\bar{A}_i^T + \bar{B}Z + Z^T\bar{B}^T & * & * \\ \bar{B}_w^T & -\gamma^2 I & * \\ \bar{C}_z X & 0 & -I \end{bmatrix} < 0, \tag{4.9}$$

where $i = 1, 2, 3, 4$ and the controller gain $K = ZX^{-1}$.

4.1.1.6 Pole-placement criteria

Here, we consider the placement of closed-loop poles in a desired LMI region [12] through state feedback control. Though the controller based on $\mathcal{L}_2$ performance criteria yields a good robust performance, the desired transient performance is however, lacking. The location of closed-loop poles guaranteeing minimum α and ζ can bring about a significant improvement in the system transient response. The following result [12] is used here for controller design.

Theorem 4.2 *[12] The closed-loop poles of system (4.8) are placed in the region $\mathcal{D}_C(\alpha,\theta)$ if, for a scalar α, there exist matrices $X>0$ and Z such that the below LMI problem has a feasible solution.*

$$\begin{bmatrix} (\bar{\Xi}_i+\bar{\Xi}_i^T+2\alpha X)\sin\theta & * \\ (\bar{\Xi}_i^T-\bar{\Xi}_i)\cos\theta & (\bar{\Xi}_i+\bar{\Xi}_i^T+2\alpha X)\sin\theta \end{bmatrix} < 0, \tag{4.10}$$

where $i=1,2,3,4$ $\bar{\Xi}_i=\bar{A}_iX+\bar{B}Z$. $\mathcal{D}_C(\alpha,\theta)$ represents an LMI region corresponding to minimum α and ζ as shown in Fig.1.5.

4.1.1.7 Controller design

The robust PI controller designed with simple $\mathcal{L}_2$ and pole placement criteria (4.9) and (4.10) fails to provide the desired set point tracking due to large values of gains that lead to saturation of the control input. Therefore, two more conditions are considered to obtain reduced gain from the feasible set satisfying (4.9) and (4.10). The additional conditions introduced for the controller design are, following [169], as,

$$\begin{bmatrix} \alpha_1 I & * \\ Z & I \end{bmatrix} > 0 \; and \; \begin{bmatrix} \beta I & * \\ I & X \end{bmatrix} > 0. \tag{4.11}$$

The first one satisfies the bound $Z^TZ \leq \alpha_1 I$ and the second one satisfies $X^{-1} \leq \beta I$. Combinedly, the computed control gain $K=ZX^{-1}$ is reduced. Following the above, the controller is designed using the below optimization problem:

$$\begin{aligned} &\text{Minimize } \alpha_1+\lambda\beta \\ &\text{subject to (4.9), (4.10), (4.11), } X>0, \end{aligned} \tag{4.12}$$

where λ is a scalar weighting factor for the multi-objective optimization problem.

4.1.1.8 Design tests on a laboratory setup

The design technique is demonstrated through the implementation on a coupled tank system in real-time and the corresponding results are presented in this section. A coupled tank experimental setup comprises two tanks, pressure sensors, tank level scale (in cm), disturbance probe and a dc pump motor that supplies water to tank 1. The setup is shown in Fig. 4.3. The values of the parameters are provided in Table 4.1.

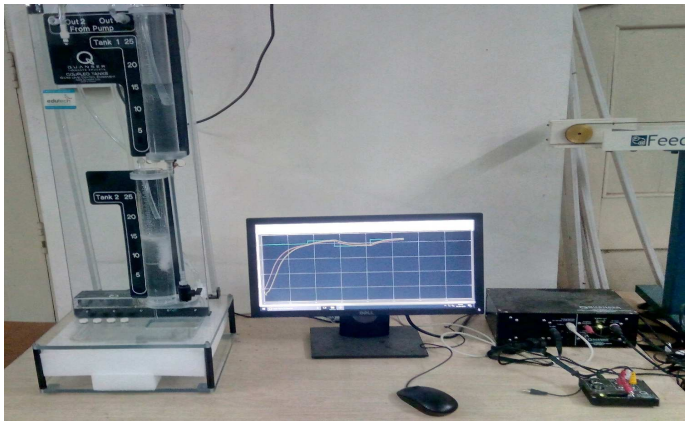

Figure 4.3: Laboratory Experimental Setup

4.1.1.9 Experimental results

For the proposed design, we consider the variation in water levels as $h_1(cm) \in [5,\ 20]$ and $h_2(cm) \in [5,\ 20]$. Then, the uncertain parameters $\rho_1 \in [9.90, 19.80]$ and $\rho_2 \in [9.90, 19.80]$. Based on this, one can obtain the system matrices of the dynamical model (4.7) with polytopic uncertainties as:

$$A_1 = \begin{bmatrix} -0.005 & 0 \\ 0.005 & -0.005 \end{bmatrix},\ A_2 = \begin{bmatrix} -0.005 & 0 \\ 0.005 & -0.0101 \end{bmatrix}, A_3 = \begin{bmatrix} -0.0101 & 0 \\ 0.0101 & -0.005 \end{bmatrix},$$
$$A_4 = \begin{bmatrix} -0.0101 & 0 \\ 0.0101 & -0.0101 \end{bmatrix}, B = \begin{bmatrix} 0.2126 \\ 0 \end{bmatrix},\ B_w = B,\ C_z = [1\ 1]$$

The $\mathcal{L}_2$ state feedback PI controller is designed by solving the optimization problem (4.12) with parameters $\alpha = 0.01$, $\theta = 50°$, $\gamma = 0.2$ and weighting factor chosen as $\lambda = 15$. The same is implemented on the real-time plant. Although LMI conditions are computationally complex to solve, they are numerically easily tractable and the solution can be obtained using LMI Control Toolbox of MATLAB [158].

A comparative study is done for a square input with peak to peak amplitude of 4 units and the various state and control input responses are demonstrated. The existing algorithms used for comparison is the conventional PI controller. Note that this controller design is carried out using the linearization around an operating point, hence it uses an approximate model of the actual system. Fig. 4.4 and Fig. 4.5 show a comparison of the tracking response for water level in tank 1 and tank 2 respectively. The responses clearly demonstrate the better tracking response of the proposed robust PI controller compared to the conventional design. Also, the transient response for the latter design is better

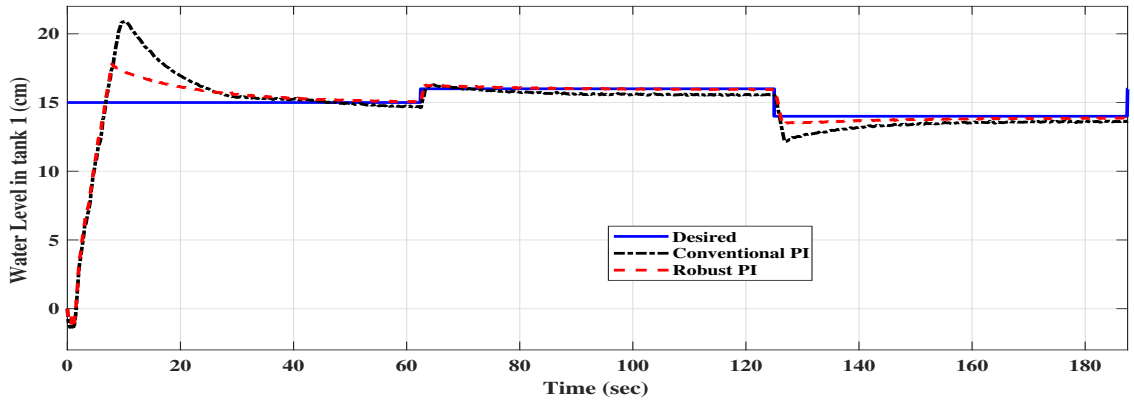

Figure 4.4: Time variation of water level in Tank 1 (h_1)

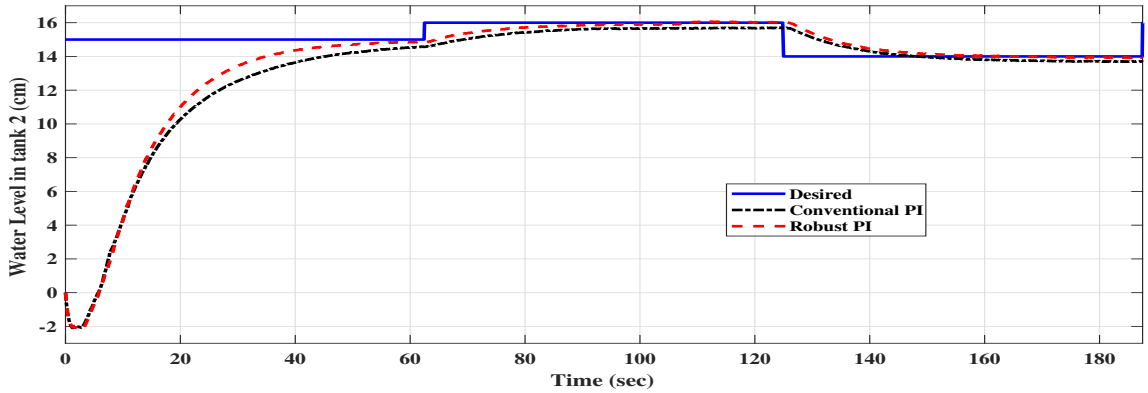

Figure 4.5: Time variation of water level in Tank 2 (h_2)

Table 4.2: Controller gains, IAE and ISE performance for different controllers

’ Controllers	Controller gain	IAE		ISE	
		Tank 1	Tank 2	Tank 1	Tank 2
Conventional PI [167]	$K_{p1} = 7.2152,\ K_{p2} = 9.1061$ $K_{i1} = 5.0934,\ K_{i2} = 1.7436$	50.15	32.34	37.78	24.81
Robust PI	$K_{p1} = 20.2916,\ K_{p2} = 20.2966,$ $K_i = 1.0039$	14.84	24.44	5.85	21.22

than the former. Additionally, the control input responses are compared in Fig. 4.6 and Fig. 4.7. From the Figures, it is observed that comparatively similar control efforts are required for setpoint tracking of tanks in both the design methods. Note that the control inputs are oscillatory rather than chattering due to the coupling effect between different states as is clearly visible from the zoomed out views embedded in the figures.

Table 4.3: Time domain performance for different controllers

Controllers	Rise time (sec)	Maximum overshoot (%)	Settling time (sec)	Steady state error (cm)
Conventional PI [167] (Tank 1)	6.8	39.33	39	0.5
Conventional PI [167] (Tank 2)	30.6	0	112	0.31
Robust PI (Tank 1)	6.7	18.67	33	0.04
Robust PI (Tank 2)	25.6	0	48	0.02

The values of controller gains and error performance with two different criteria (Integral Square Error (ISE) and Integral Absolute Error (IAE)), for different controllers are computed and provided in Table 4.2. A performance analyses of the time domain specifications is shown in Table 4.3. The criteria considered for calculating the rise time is 10-90% for overdamped system and 0-100% for underdamped system. The settling time is calculated according to 2% tolerance criteria. It can be clearly observed from both that the proposed design scores over the other with a lower ISE and IAE, rise time, maximum percentage overshoot, settling time and a negligible steady state error.

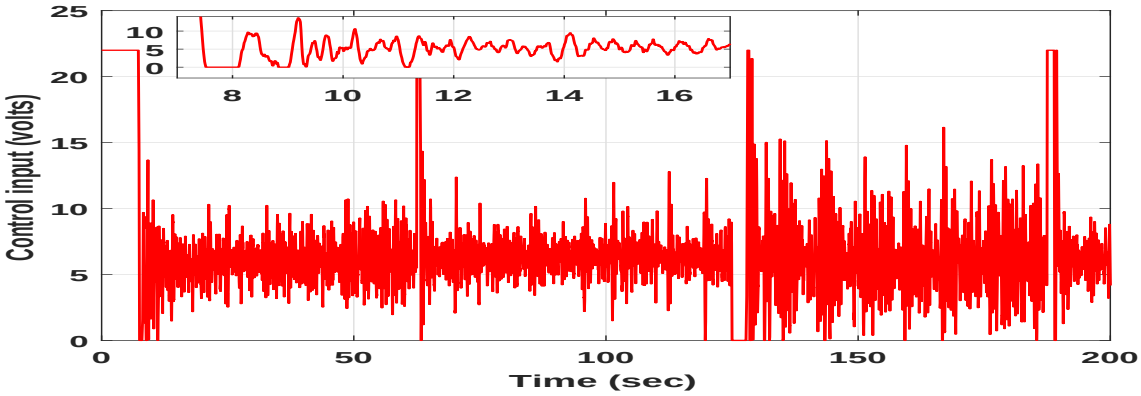

Figure 4.6: Time variation of control input (Conventional PI controller)

4.1.2 Twin Rotor MIMO System: 2-DOF Helicotper

We now consider our next example, which is a Twin Rotor MIMO system (TRMS). The TRMS is a complex nonlinear and multivariate unstable aero-dynamical system [170,171], characterized by significant cross-coupling between the two rotors which are driven by

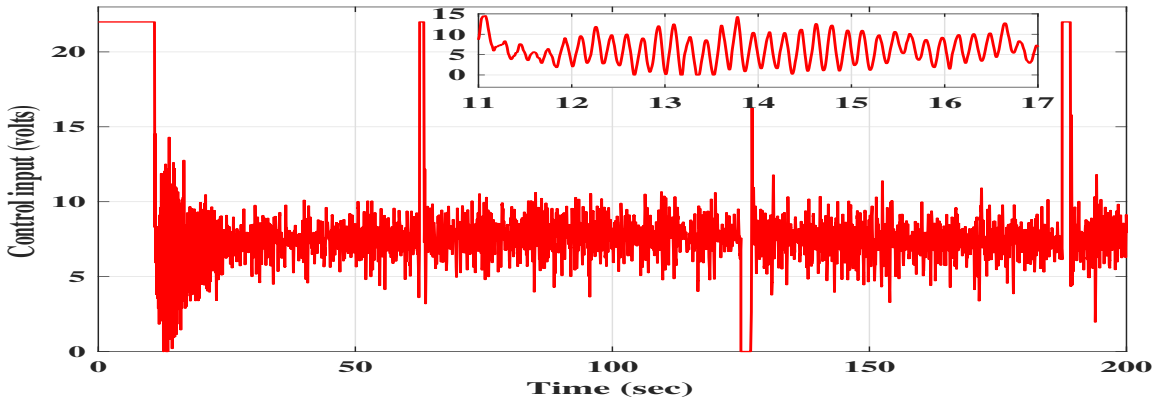

Figure 4.7: Time variation of control input (Proposed PI controller)

electric motors and are free to rotate in horizontal and vertical planes, respectively. A helicopter control system is a prototype of TRMS.

Now, on the same lines as the coupled tank system, we capture the nonlinear variations arising in the system through a polytopic model so that a linear controller [155] can be designed guaranteeing appropriate system performance. The nonlinear dynamics of a TRMS are represented in a linear polytopic form not involving any approximation of the higher order terms. A robust state feedback PI controller has been designed based on LMIs for the 2-DOF helicopter model (an example case of the TRMS). The designed controller has a decentralized structure which involves diagonal Z and X matrices, which can be easily incorporated in the LMI programs. This is helpful in removing the cross-coupling between the pitch and yaw plane dynamics that improves tracking control of the MIMO system. By placing the closed-loop poles in a desired LMI region, the transient response is satisfactorily improved, thereby ensuring a minimum α and ζ. The designed controller is tested on a 2-DOF helicopter system [150] in real time.

4.1.2.1 Mathematical modeling

Consider a twin rotor MIMO system whose free body diagram is shown in Fig. 4.8. It consists of two motor-propeller assemblies; the one in the front controls the elevation angle of the nose over the pitch axis while the other at the tail guides the rotational motion about the yaw axis. It is assumed that the pitch and yaw thrust forces, i.e., F_p and F_y always remain positive when pitch angle and yaw angle increase ($\theta_1 > 0$, $\theta_2 > 0$). The parameters of the 2-DOF helicopter [150] are given in the Table 4.4 .

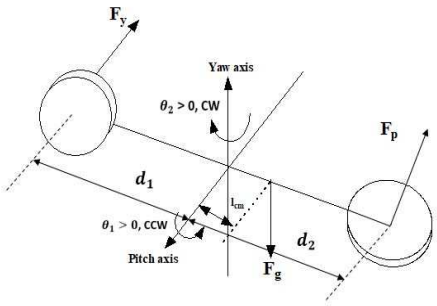

Figure 4.8: Free body diagram of a generalised TRMS

Table 4.4: System Value Parameters

Symbol	Description	Value	Unit
K_{pp}	Torque constant for pitch assembly	0.204	N-m/V
K_{yy}	Torque constant for yaw assembly	0.072	N-m/V
B_p	Damping factor about pitch axis	0.800	N/V
B_y	Damping factor about yaw axis	0.318	N/V
J_p	Inertial Moment about pitch axis	0.0384	kg-m^2
J_y	Inertial Moment about yaw axis	0.0432	kg-m^2
M_p	Total mass about pitch axis	0.633	kg
M_y	Total mass about yaw axis	0.667	kg
M_h	Helicopter mass	1.3872	kg
K_{py}	Cross-torque constant, acting along pitch axis from yaw motor	0.0068	N-m/V
K_{yp}	Cross-torque constant, acting along yaw axis from pitch motor	0.0219	N-m/V
d_1	Distance of pitch motor from hinge, along the helicopter body	0.186	m
d_2	Distance of yaw motor from hinge, along the helicopter body	0.186	m

$$
\begin{aligned}
\dot{x}_1 =& x_3,\ \dot{x}_2 = x_4, \\
\dot{x}_3 =& \frac{-M_y d_2^2 x_4^2 cos(x_1) sin(x_1) - M_p d_1^2 x_4^2 cos(x_1) sin(x_1)}{M_p d_1^2 + M_y d_2^2 + J_p} \\
&+ \frac{\tau_1 - B_p x_3 + M_y g d_2 cos(x_1) - M_p g d_1 cos(x_1)}{M_p d_1^2 + M_y d_2^2 + J_p} \\
\dot{x}_4 =& \frac{\tau_2 - B_y x_4 + 2M_p d_1^2 x_3 x_4 cos(x_1) sin(x_1)}{M_p d_1^2 + M_y d_2^2 + J_y} + \frac{2M_y d_2^2 x_3 x_4 cos(x_1) sin(x_1)}{M_p d_1^2 + M_y d_2^2 + J_y}
\end{aligned} \tag{4.13}
$$

The state-space expression of the nonlinear dynamical model [150] is given by (4.13). Here, x_1, x_2, x_3 and x_4 are the states of the system representing pitch angle (θ_1), yaw angle (θ_2), pitch velocity ($\dot{\theta_1}$) and yaw velocity ($\dot{\theta_2}$), respectively. $\tau_1 = K_{pp}V_1 + K_{py}V_2$ is the sum total of thrust torque from pitch motor and cross torque acting along the pitch axis from yaw motor, where, V_1 and V_2 are the control voltages to pitch and yaw motors. It is given as $\tau_1 = M_p d_1^2\ddot{\theta_1} + M_p d_1^2\dot{\theta_2}^2 sin\theta_1 cos\theta_1 + M_y d_2^2\ddot{\theta_1} + M_y d_2^2\dot{\theta_2}^2 cos\theta_1 sin\theta_1 + J_p\ddot{\theta_1} + M_p g d_1 cos\theta_1 - M_y g d_2 cos\theta_1 + B_p\dot{\theta_1}$. Similarly, $\tau_2 = K_{yp}V_1 + K_{yy}V_2$ is the sum total of thrust torque from yaw motor and cross torque acting along the yaw axis from pitch motor. It is given as $\tau_2 = M_p d_1^2\ddot{\theta_2}^2 cos\theta_1^2 + M_y d_2^2\ddot{\theta_2}^2 cos\theta_1^2 + 2M_p d_1^2\dot{\theta_1}\dot{\theta_2} cos\theta_1 sin\theta_1 - 2M_y d_2^2\dot{\theta_1}\dot{\theta_2} cos\theta_1 sin\theta_1 + J_y\ddot{\theta_2} + B_y\dot{\theta_2}$.

4.1.2.2 Polytopic model

We now represent the nonlinear TRMS model in the form of a linear parameter-varying one and thereby, as a polytopic system. We consider that the pitch angle (x_1) is uncertain but bounded, i.e., $x_1 \in [\underline{x}_1, \bar{x}_1]$ such that the nonlinearity due to the term $x_4 cos(x_1) sin(x_1)$ is taken as an uncertain parameter (ρ), which varies between ρ_{min} and ρ_{max}. The boundary values up to which the yaw velocity represented by the state x_4 varies is considered to be known. Also, we have assumed that all the other system parameters are well known. The nonlinear model (4.13) can be expressed as a linear one:

$$\dot{x}(t) = A(\rho)x(t) + Bu(t) + B_w w(t),\ z(t) = C_z x(t), \tag{4.14}$$

where $x(t) \in \mathbb{R}^4$ represents the state vector, $u(t) \in \mathbb{R}^2$ and $z(t) \in \mathbb{R}^4$ are the control input and controlled output of the system, respectively. Further, $w(t) \in \mathbb{R}^2$ is the disturbance input. $A(\rho)$ is the parameter dependent system matrix. $A(\rho)$, B, B_w and C_z matrices are given by

$$A(\rho) = \begin{bmatrix} 0 & 0 & 1 & 0 \\ 0 & 0 & 0 & 1 \\ 0 & 0 & -\frac{B_p}{\bar{J}_p} & -a_1\rho \\ 0 & 0 & a_2\rho & -\frac{B_y}{\bar{J}_y} \end{bmatrix}, B = \begin{bmatrix} 0 & 0 \\ 0 & 0 \\ \frac{K_{pp}}{\bar{J}_p} & \frac{K_{py}}{\bar{J}_p} \\ \frac{K_{yp}}{\bar{J}_y} & \frac{K_{yy}}{\bar{J}_y} \end{bmatrix}, B_w = \begin{bmatrix} 0 & 0 \\ 0 & 0 \\ w_1 & 0 \\ 0 & 0 \end{bmatrix}, C_z = I_{4\times 4},\ \rho \in [\rho_{min},\ \rho_{max}],$$

where $\bar{J}_p = M_p d_1^2 + M_y d_2^2 + J_p, \bar{J}_y = M_p d_1^2 + M_y d_2^2 + J_y,\ a_1 = \frac{(M_y d_2^2 + M_p d_1^2)}{\bar{J}_p},\ a_2 = \frac{2(M_y d_2^2 + M_p d_1^2)}{\bar{J}_y}, w_1 = \frac{(M_y g d_2 - M_p g d_1) cos(x_1)}{\bar{J}_p},\ \rho = x_4 sin(x_1) cos(x_1)$. Note that similar assumptions as in Assumption 2 follow again but with 2 vertices of the polytope. Further, the

closed-loop TRMS block diagram is shown in Fig. 4.9. The main aim now, is to design a robust state feedback decentralized PI controller for tracking control of the TRMS. All system states are assumed to be measurable at the output.

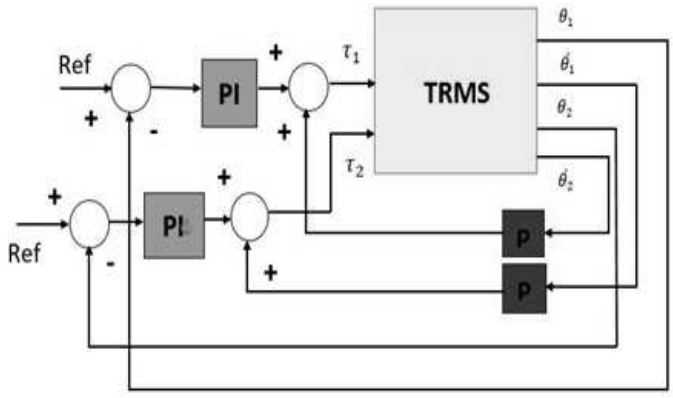

Figure 4.9: Block Diagram of the closed-loop system

4.1.2.3 Design tests on TRMS setup

The design approach is applied to a 2-DOF helicopter system in real-time and the corresponding results are presented in this section. The experimental setup of a Quanser

Figure 4.10: Experimental setup

make 2-DOF helicopter [150] is shown in Fig. 4.10 with the following specifications. It consists of two brushless DC motors responsible for actuating the motion along pitch and yaw axis separately. The pitch motor (Pittman Model 9234) has an electrical resistance, current-torque constant and a peak voltage of 0.83 Ω, 0.0182 Nm/A and 22 V respectively, without damage. The yaw motor (Faulhaber Series 2842) has a terminal resistance and a

current-torque constant of 1.6 Ω and 0.0109 Nm/A, respectively. Further, the pitch and yaw propeller assemblies comprise the Graupner 20/15 cm or 8/6" propellers, directly mounted to the motor shaft with thrust-force constants of 0.104 N/V and 0.43 N/V, respectively. The position measurements are taken by two optical encoders, connected to a data-acquisition board. The quadrature mode resolution of the pitch and yaw encoders are 4096 and 8192 counts per revolution, with effective position resolutions of 0.0879° and 0.0439° about the pitch and yaw axis, respectively. Using position measurements, the velocity is computed via a derivative filter of suitable corner frequency to mitigate its sensitivity effects towards measurement noise present in the system.

4.1.2.4 Design of PI controller

For the proposed design, we consider the variation in the pitch angle as $x_1 \in [-15°,\ 15°]$ and maximum value which the trajectory of the state x_4 can take is 3 deg/sec. Then, the uncertain parameter ρ lies in between -0.75 and 0.75. Based on this, one can obtain the system matrices of the dynamical model (4.14) with polytopic uncertainties as:

$$A_1 = \begin{bmatrix} 0 & 0 & 1 & 0 \\ 0 & 0 & 0 & 1 \\ 0 & 0 & -9.2603 & -0.3905 \\ 0 & 0 & 0.7809 & -3.4872 \end{bmatrix}, B = \begin{bmatrix} 0 & 0 \\ 0 & 0 \\ 2.3614 & 0.0787 \\ 0.2402 & 0.7896 \end{bmatrix}, A_2 = \begin{bmatrix} 0 & 0 & 1 & 0 \\ 0 & 0 & 0 & 1 \\ 0 & 0 & -9.2603 & 0.3905 \\ 0 & 0 & -0.7809 & -3.4872 \end{bmatrix},$$

$$B_w = \begin{bmatrix} 0 & 0 & 0.7181 & 0 \\ 0 & 0 & 0 & 0 \end{bmatrix}^T, C_z = I_{4\times 4},\ \rho \in [-0.75,\ 0.75]$$

The $\mathcal{L}_2$ based state feedback PI controller is designed by considering $C_a = \begin{bmatrix} 1 & 0 & 0 & 0 \\ 0 & 1 & 0 & 0 \end{bmatrix}$ and solving the optimization problem (4.12) given in previous section with parameters $\alpha = 0.5$, $\theta = 20°$, $\gamma = 0.05$ and weighting factor $\lambda = 10$. The same is implemented on the real-time plant. The solution of the LMIs is obtained using LMI Control Toolbox of MATLAB [158]. A comparative study is done for a square input with peak-peak amplitude of 4° and the various state and control input responses are demonstrated. The existing algorithms used for comparison are Optimal LQR-Integral method [150] and Adaptive Particle Swarm Optimization (APSO) [172].

Fig. 4.11 shows a comparison of the pitch angle tracking performance between the

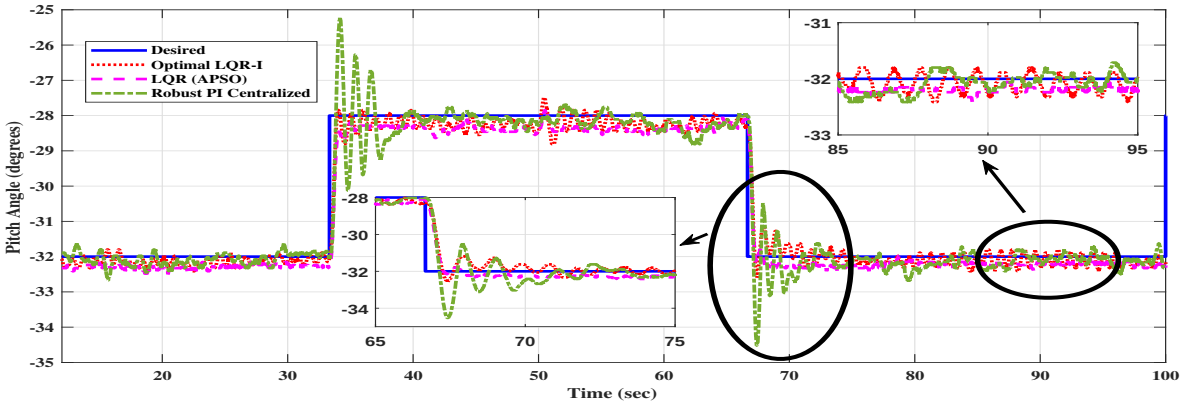

Figure 4.11: Time variation of pitch angle

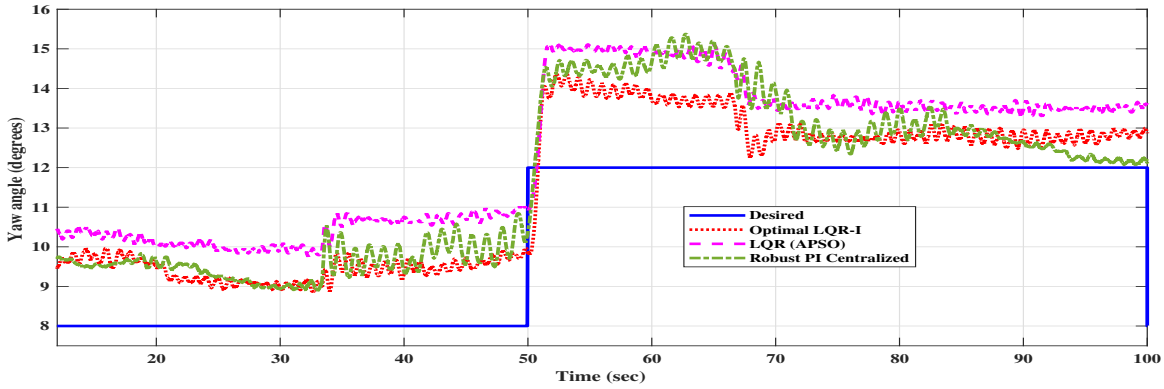

Figure 4.12: Time variation of yaw angle

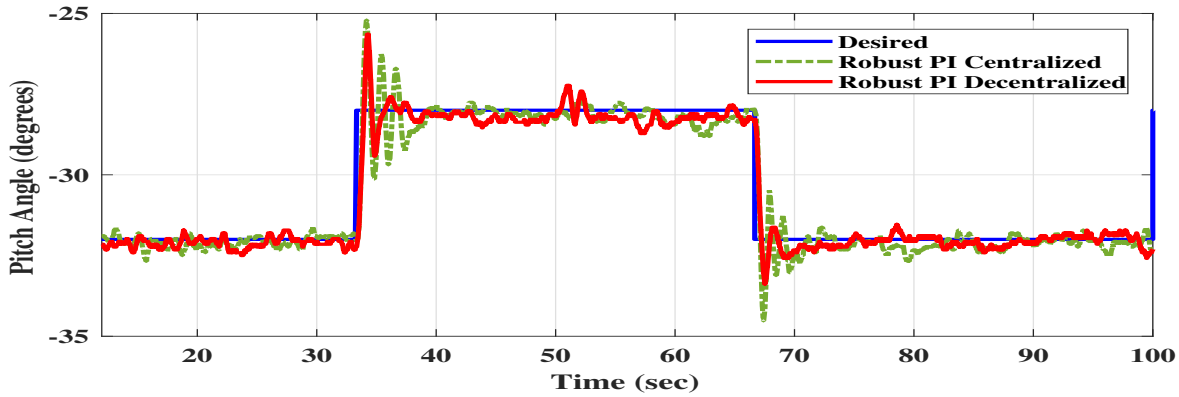

Figure 4.13: Comparison of time variation of pitch angle of Robust PI for centralized and decentralized cases

centralized robust PI controller and those mentioned above. A similar comparison has been done for yaw angle tracking performance in Fig. 4.12. As can be seen from the magnified views with clarity, the centralized PI controller design shows a good tracking

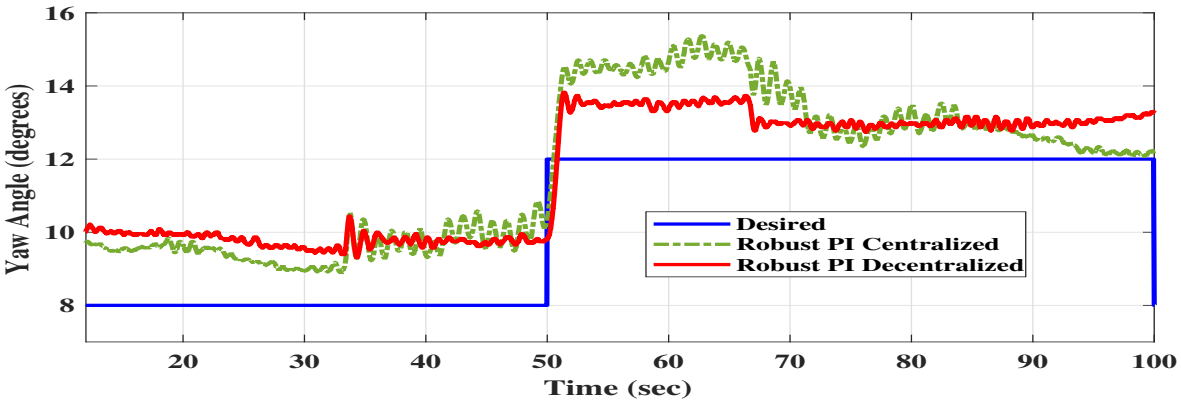

Figure 4.14: Comparison of time variation of yaw angle of Robust PI for centralized and decentralized cases

response of the pitch response. Similarly the yaw response tracks the set point significantly well along with an improved transient response compared to other controllers.

Additionally, the same robust controller design method is used to design a decentralized controller as in Fig. 4.13 and Fig. 4.14. As stated earlier, the decentralized controller design involves diagonal Z and X matrices, which can be easily incorporated in the LMI programs. The corresponding responses are shown in Figs. 7-12 in comparison to the centralized controller. As is observed in Fig. 4.13, the pitch tracking transient response is good, with an equally good steady state response for the decentralized controller. Further, Fig. 4.14 shows a better tracking response in yaw angle. The decentralized controller provides a better response against cross-couplings since it prevents any additional interactions entering via the control channel. Also, Fig. 4.15 and Fig. 4.16 show a comparison between the control inputs for the pitch and yaw angles for the centralized and decentralized controllers. It can be easily seen that the inputs for both the planes are less aggressive for the decentralized case, thus reducing the amount of control effort required to track the desired input efficiently. The values of controller gains and error performance with two different criteria (Integral Square Error (ISE) and Integral Absolute Error (IAE)) with sampling time of 2 $msec$, for different controllers are computed and provided in Table 4.5 and 4.6, respectively. It can be easily observed that the robust controllers performs better than the others.

Table 4.5: Different Controller Gains

Controllers	Controller Gain $[K_p \; K_I]$
LQR-I [150]	$\begin{bmatrix} 18.9 & 1.98 & 7.49 & 1.53 & 7.03 & 0.77 \\ -2.22 & 19.4 & -0.45 & 11.9 & -0.77 & 7.03 \end{bmatrix}$
LQR-I (APSO) [172]	$\begin{bmatrix} 19.24 & 2.17 & 9.17 & 1.27 & 10.37 & 1.39 \\ -1.79 & 14.29 & -0.31 & 6.21 & -0.83 & 7.63 \end{bmatrix}$
Robust PI Centralised	$\begin{bmatrix} 19.91 & 1.36 & 3.96 & 0.72 & 9.10 & 0.63 \\ -4.50 & 24.82 & -0.63 & 7.97 & -1.93 & 10.03 \end{bmatrix}$
Robust PI Decentralised	$\begin{bmatrix} 11.79 & 0 & 2.28 & 0 & 3.48 & 0 \\ 0 & 22.88 & 0 & 6.85 & 0 & 7.04 \end{bmatrix}$

Table 4.6: Error Performance for Different Controllers

Controllers	IAE		ISE	
	Pitch	Yaw	Pitch	Yaw
LQR-I [150]	14.97	81.29	9.6	173.24
LQR-I (APSO) [172]	20.70	131.50	12.60	409.05
Robust PI Centralised	15.87	47.28	11.31	89.91
Robust PI Decentralised	13.39	30.67	10.91	61.11

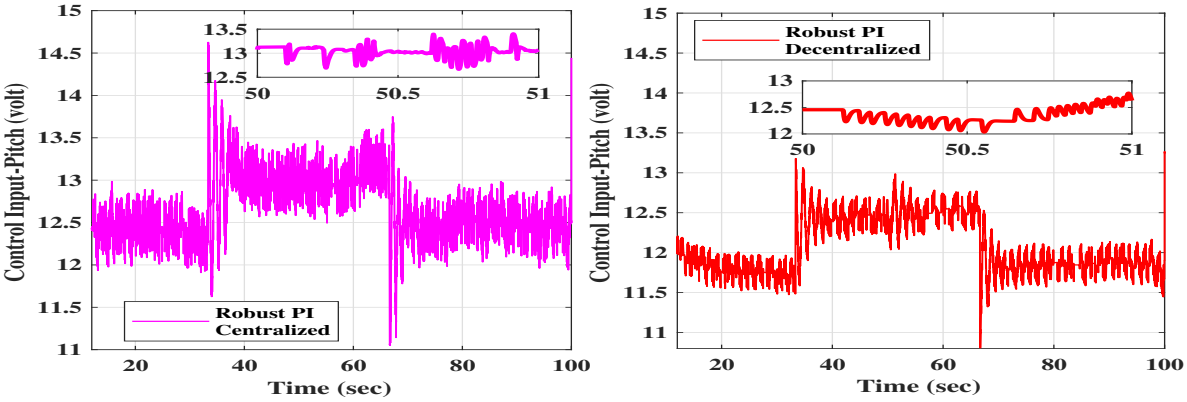

Figure 4.15: Time variation of control input for pitch angle

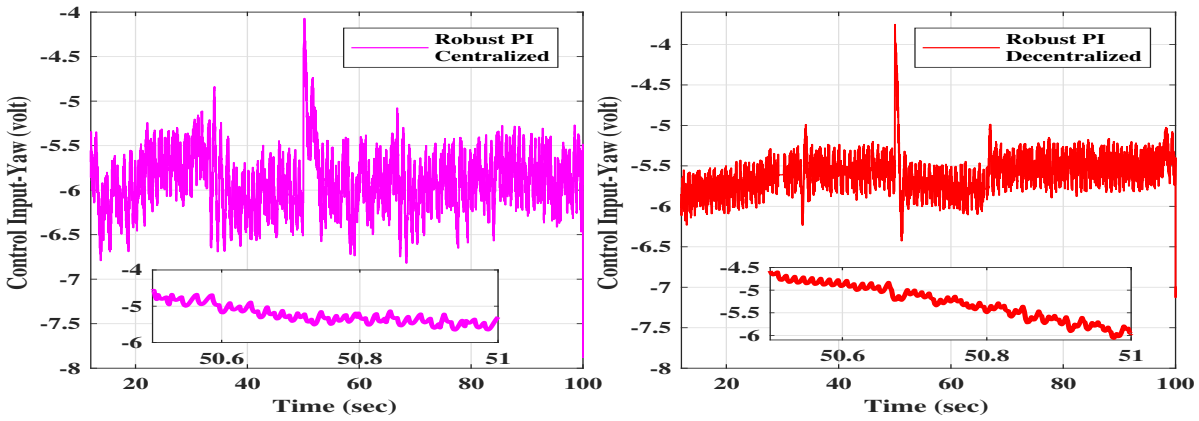

Figure 4.16: Time variation of control input for yaw angle

4.1.3 Quasi-LPV PI control of TRMS subject to actuator saturation

Next, we represent the TRMS system via a quasi-LPV representation in this section and design a controller by incorporating more practical constraints such as the actuator saturation.

Linear parameter varying plants are linear dynamical systems [173] whose state space matrices are known functions of time varying parameters (scalar parameter δ_t, in this case). The generalized LPV model in state space form incorporating actuator saturation nonlinearity is given as

$$\begin{aligned} \dot{x}(t) &= A(\delta_t)x(t) + B(\delta_t)sat\{u(t)\} + B_w(\delta_t)w(t) \\ z(t) &= C_z(\delta_t)x(t) \end{aligned} \tag{4.15}$$

where $x(t) \in \mathbb{R}^n$ is the state vector, $u(t) \in \mathbb{R}^m$, $z(t) \in \mathbb{R}^{p_1}$ and $w(t) \in \mathbb{R}^{m_2}$ represent the input vector, controlled output and input disturbance respectively. $A(\delta_t), B(\delta_t), C(\delta_t)$ and $D(\delta_t)$ are parameter varying matrices with suitable dimensions. The saturation function $sat\{.\} : \mathbb{R}^m \to \mathbb{R}^m$ and $sat\{u(t)\} = [sat\{u_1(t)\}, \cdots, sat\{u_m(t)\}]^T$ is defined as

$$sat\{u_j(t)\} := \begin{cases} \bar{u}_j & u_j(t) \geq \bar{u}_j \\ u_j(t), & u_j(t) \in [-\bar{u}_j, \bar{u}_j],\ j = 1, \cdots, m \\ -\bar{u}_j, & u_j(t) \leq -\bar{u}_j \end{cases} \tag{4.16}$$

where $\bar{u}_j$ is the amplitude of the j^{th} input. Note that the variable δ_t in this paper is actually dependent on state variables through the measured output. These variables thus, enter

the control loop both as parameters (in δ_t) and dynamic variables of the linearized plant. Such systems have been termed in literature as quasi-LPV, or qLPV for shorthand.

The LPV framework has been long studied for modeling and control design purpose owing to its potential applications in a variety of disciplines such as automotive systems [174], IC manufacturing [175], energy sector [176], control of induction machines [177] and power electronic control of three-phase inverters for microgrid frequency stabilization [178]. Although time variation of the varying parameter is not known in advance, it is assumed to be measurable in real-time. By exploiting this feature, the LPV framework can synthesize an automatically scheduled controller by formulating the problem into a convex setting.

Additionally, the common actuator saturation problem, applicable to almost every industrial apparatus, is the limitation of the magnitude of control signal actuation to retain the designed control action and avoid unnecessary damage of the components. Design of robust control under such actuator saturation is a challenging task since it leads to deterioration of system performance, occurrence of limit cycles, multiple equilibria and may cause instability [14, 179, 180].

Motivated by the merits of LPV control and above-mentioned problems of TRMS controller design, here, in this section, we propose an effective approach based on the LPV control design under actuator saturation. The system is represented as a qLPV polytopic one by considering the nonlinear terms as parametric uncertainties and without ignoring any higher order dynamics. In conjunction to this, input actuator saturation has been handled using, again, a polytopic formulation to restrict the controller gains within desirable limits using a contractively invariant set under linear feedback. Based on the concept of quadratic $\mathcal{L}_2$ performance, the synthesis problem is formulated in a convex setting. The qLPV PI controller is designed both in the centralized and the decentralized framework. The latter resembles a diagonal controller so that the process outputs follow the corresponding reference signals while maintaining the cross interactions within limits that improves tracking control of the MIMO system. In addition, the decentralized structure involves diagonal Z and X matrices, which can be easily incorporated in the LMI programs. Satisfactory transient response is ensured by placing the closed-loop eigenvalues in a sector based LMI region. The motivation behind pole placement lies in the fact that eigenvalues of a time-varying system have direct impact on the transient response

of the overall system. An experimental demonstration on a laboratory prototype is used to illustrate the benefits of the proposed design. A comparison of the proposed qLPV approach is carried out with the methods employing Jacobian linearized models.

4.1.3.1 qLPV model

This section discusses the qLPV polytopic form of the nonlinear model in (4.13).

Definition 1 (qLPV Polytopic System [181]) *A qLPV system is referred to as polytopic if the state matrices are defined as in* (4.15)*, where δ_t, which is the time-varying parameter, ranges over a fixed polytope and the matrices $A(.)$, $B(.)$, $C(.)$ and $D(.)$ depend affinely on δ_t.*

We consider that the pitch angle (x_1) is measurable in real-time with $x_1 \in [\underline{x}_1, \bar{x}_1]$ and the nonlinear term $x_4 cos(x_1) sin(x_1)$ represents the time varying parameter (δ_t). The boundary values enclosing the yaw velocity (x_4) are considered to be known. The reason behind the choice of the aforementioned term as δ_t is because it is common to both the states x_3 and x_4. Finally, the nonlinear model (4.13) can be written in the qLPV polytopic form under input actuator saturation as:

$$\begin{aligned} \dot{x}(t) &= A(\delta_t)x(t) + B_w w(t) + B sat\{u(t)\}, \\ z(t) &= C_z x(t), \end{aligned} \tag{4.17}$$

where $A(\delta_t)$ is the parameter dependent matrix. Also, $sat\{u(t)\} = [sat\{u_1(t)\}, sat\{u_2(t)\}]^T$. Using parameters from Table 4.4, the matrices $A(\delta_t)$, B, B_w and C_z can be calculated as

$$A(\delta_t) = \begin{bmatrix} 0 & 0 & 1 & 0 \\ 0 & 0 & 0 & 1 \\ 0 & 0 & -\frac{B_p}{\bar{J}_p} & -\frac{(M_y d_2^2 + M_p d_1^2)}{\bar{J}_p}\delta_t \\ 0 & 0 & \frac{2(M_y d_2^2 + M_p d_1^2)}{\bar{J}_y}\delta_t & -\frac{B_y}{\bar{J}_y} \end{bmatrix}, B = \begin{bmatrix} 0 & 0 \\ 0 & 0 \\ \frac{K_{pp}}{\bar{J}_p} & \frac{K_{py}}{\bar{J}_p} \\ \frac{K_{yp}}{\bar{J}_y} & \frac{K_{yy}}{\bar{J}_y} \end{bmatrix},$$

$$B_w = \begin{bmatrix} 0 \\ 0 \\ \frac{(M_y g d_2 - M_p g d_1)}{\bar{J}_p} \\ 0 \end{bmatrix}, C_z = I_{4\times 4},\ \delta_t \in [\underline{\delta_t},\ \bar{\delta_t}],\ w(t) = cos(x_1).$$

Fact 6 *1. The system matrix $A(\delta_t)$ is assumed to be continuous and bounded and real-time measurements of δ_t are available.*

2. *The parameter $\delta_t \in [\underline{\delta_t},\ \bar{\delta_t}]$ varies in a parameter space, which is a polytope given as:*

$$\delta_t \in Co\{\zeta_1, \zeta_2\} := \left\{ \sum_{i=1}^{2} \epsilon_i \zeta_i : \epsilon_i \geq 0, \sum_{i=1}^{2} \epsilon_i = 1 \right\}.$$

The vertices of the polytope for the matrix $A(\delta_t)$ correspond to a set $\{A_1, A_2\}$, where A_1, A_2 are the extrema of a convex polytope. Thus,

$$A(\delta_t) \in Co\{A_1, A_2\} := \left\{ \sum_{i=1}^{2} \epsilon_i A_i,\ \epsilon_i \geq 0,\ \sum_{i=1}^{2} \epsilon_i = 1 \right\}. \tag{4.18}$$

Taking into account Fact 6, system (4.17) can be represented in polytopic form as:

$$\begin{bmatrix} A(\delta_t) & B & B_w \\ C_z & 0 & 0 \end{bmatrix} = \sum_{i=1}^{2} \epsilon_i \begin{bmatrix} A(\zeta_i) & B & B_w \\ C_z & 0 & 0 \end{bmatrix} \tag{4.19}$$

Note that although the system (4.17) has a linearized appearance, it still fully accommodates the nonlinear model without any approximation as opposed to conventional linearization schemes using Taylor's polynomial approximations.

4.1.3.2 $\mathcal{L}_2$ based PI controller design

In this section, we propose a decentralised robust state feedback qLPV PI controller for the qLPV plant of the previous section for tracking control of TRMS. A block schematic of the closed-loop system is shown in Fig. 4.17. The qLPV TRMS model block in the figure represents the state equation given by (4.17). The P and I bocks represent the gain values (K_p and K_I, respectively) applied to the state error and are determined below using Problem 1. It is assumed that all the states are available for measurement at the output.

4.1.3.3 PI controller design

The PI controller for the system (4.17) is given as

$$u(t) = K_p(\delta_t)x(t) + K_I(\delta_t) \int_0^t y_t(\tau)d\tau,\ y_t(t) = C_a x(t) \tag{4.20}$$

where $C_a = \begin{bmatrix} I_{2\times 2} & 0_{2\times 2} \end{bmatrix}$ involves only the pitch and the yaw angles for tracking. $K_p(\delta_t) \in \mathbb{R}^{2\times 4}, K_I(\delta_t) \in \mathbb{R}^{2\times 2}$ are the controller gain matrices of the PI controller which are to be

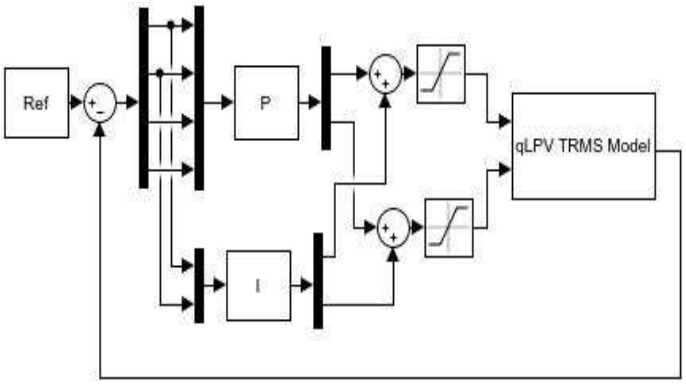

Figure 4.17: Block schematic of the closed-loop model

designed. Equation (4.20) can be further written as

$$u(t) = \begin{bmatrix} K_p(\delta_t) & K_I(\delta_t) \end{bmatrix} \begin{bmatrix} x(t) \\ \int_0^t y_t(\tau)d\tau \end{bmatrix}, \quad y_t(t) = C_a x(t). \tag{4.21}$$

Consider the augmented states for controller design in a new state vector $\tilde{x}(t)$ as

$$\tilde{x}(t) = \begin{bmatrix} x^T(t) & \int_0^t y_t^T(\tau)d\tau \end{bmatrix}^T.$$

Now using (4.21) in (4.17), the new state dynamics of $\bar{x}(t)$ is given as

$$\begin{bmatrix} \dot{x}(t) \\ y_t(t) \end{bmatrix} = \begin{bmatrix} A(\delta_t) & 0 \\ C_a & 0 \end{bmatrix} \begin{bmatrix} x(t) \\ \int_0^t y_t(\tau)d\tau \end{bmatrix} + \begin{bmatrix} Bsat\{u(t)\} \\ 0 \end{bmatrix} + \begin{bmatrix} B_w w(t) \\ 0 \end{bmatrix}, z(t) = \begin{bmatrix} C_z & 0 \end{bmatrix} \begin{bmatrix} x(t) \\ \int_0^t y_t(\tau)d\tau \end{bmatrix},$$

which can be further rewritten as

$$\begin{aligned} \dot{\tilde{x}}(t) &= \bar{A}(\delta_t)\tilde{x}(t) + \bar{B}sat\{u(t)\} + \bar{B}_w w(t), \\ z(t) &= \bar{C}_z \tilde{x}(t), \end{aligned} \tag{4.22}$$

where $\bar{A}(\delta_t)$, $\bar{B}$, $\bar{B}_w$ and $\bar{C}_z$ represent the augmented system matrices of the closed-loop system and are given by $\bar{A}(\delta_t) = \begin{bmatrix} A(\delta_t) & 0 \\ C_a & 0 \end{bmatrix}$, $\bar{B} = \begin{bmatrix} B \\ 0 \end{bmatrix}$, $\bar{B}_w = \begin{bmatrix} B_w \\ 0 \end{bmatrix}$, $\bar{C}_z = \begin{bmatrix} C_z & 0 \end{bmatrix}$. Further, $K(\delta_t) = \begin{bmatrix} K_p(\delta_t) & K_I(\delta_t) \end{bmatrix}$. Note also that the controller (4.20) can be viewed as a PID controller, assuming the outputs of the system as the pitch and the yaw angles (x_1, x_2, respectively) and which is also denoted by $y_t(t)$ in (4.20). Then, $u(t)$ in (4.20) can be written as

$$\begin{aligned} u(t) =& K_P(\delta_t)y_t(t) + K_D(\delta_t)\dot{y}_t(t) + K_I(\delta_t)\int_0^t y_t(\tau)d\tau, \\ =& K_{PD}(\delta_t)x(t) + K_I(\delta_t)\int_0^t y_t(\tau)d\tau. \end{aligned}$$

Then, the $K_p(\delta_t)$ in (4.20) is equivalent to a proportional-derivative gain matrix $K_{PD}(\delta_t) = [K_P(\delta_t) \;\; K_D(\delta_t)]$, where $K_P(\delta_t) \in \mathbb{R}^{2\times 2}$ is the proportional gain, and $K_D(\delta_t) \in \mathbb{R}^{2\times 2}$ is the derivative gain. We now state the following Bounded Real Lemma, which will be helpful in deriving the main results.

Lemma 4.3 *[3, eq. 7.27, page 110] The $\mathcal{L}_2$ gain of the system (4.17) from input $w(t)$ to output $z(t)$ is less than γ if and only if there exists matrix $X = X^T > 0$ such that*

$$\begin{bmatrix} XA(\delta_t) + A^T(\delta_t)X & * & * \\ B_w^T & -\gamma^2 I & * \\ C_z X & 0 & -I \end{bmatrix} < 0. \tag{4.23}$$

The following definition is now used to define the quadratic $\mathcal{L}_2$ performance of system (4.15).

Definition 2 *[181] The qLPV system (4.15) has quadratic $\mathcal{L}_2$ performance if and only if there exists matrix $X = X^T > 0$ such that Lemma 4.3 is satisfied for all admissible values of δ_t.*

Then, the Lyapunov function $V(x(t)) = x(t)^T P x(t),\; P = X^{-1}$ establishes asymptotic stability if the $\mathcal{L}_2$ gain from $w(t)$ to $z(t)$ is bounded by γ, i.e.,

$$\sup_{admissible\ \delta_t} \; \sup_{w(t)} \frac{(\int_0^\infty z^T(t)z(t)dt)^{\frac{1}{2}}}{(\int_0^\infty w^T(t)w(t)dt)^{\frac{1}{2}}} < \gamma. \tag{4.24}$$

Remark 4.4 *The overall controller is given by a linear combination of constant matrices as $K(\delta_t) = \sum_{i=1}^{2} \sigma_i K_i = \sigma(\delta_t)K_1 + (1 - \sigma(\delta_t))K_2$, where $0 \leq \sigma_i \leq 1$ and is given as*

$$\sigma(\delta_t) = \frac{\delta_t - \underline{\delta_t}}{\bar{\delta_t} - \underline{\delta_t}} \tag{4.25}$$

and K_1, K_2 are constant initial gains obtained by solving the optimization problem described later in Theorem 4.6.

The control strategy is shown in Fig. 4.18 with the endogenous scheduling variable δ_t. Note that the variable is called endogenous because of its explicit dependence on the system states (scheduling on internal variables).

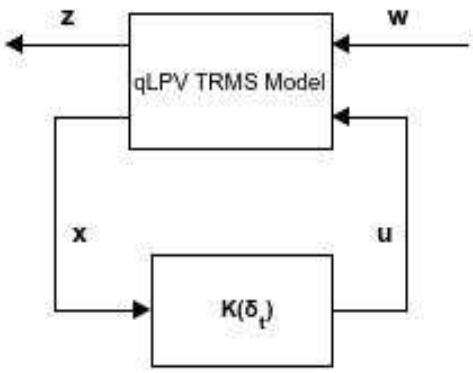

Figure 4.18: Schematic diagram of qLPV control strategy

4.1.3.4 Controller design under actuator saturation

In this section, LMI conditions for design of $\mathcal{L}_2$ based controller for the TRMS with the inclusion of actuator saturation nonlinearity is presented. We recall the following preliminaries pertaining to actuator saturation that will be used to obtain the main results.

Definition 3 *[157, Definition 3.9, page 110] A set $\mathscr{S} \in \mathbb{R}^n$ is said to be invariant if all trajectories of* (4.15) *originating from it stay within.*

Definition 4 *[182] A compact ellipsoidal convex set $\bar{\Omega}(P,1) \subset \mathscr{S}$ for P, is defined as*

$$\bar{\Omega}(P,1) := \left\{x(t) \in \mathbb{R}^n : x^T(t)Px(t) \leq 1\right\}$$

Definition 5 *[157] Let $\phi(t,x_0)$ be the state trajectories of* (4.17) *with $w(t) = 0$ and initial state x_0. The region of attraction of the origin denoted by $\mathcal{S}$ is defined as*

$$\mathcal{S} := \{x_0 \in \mathbb{R}^n : \phi(t,x_0) \to 0 \text{ as } t \to \infty\}$$

Based on the above definitions, Definition 6 and Lemma 4.5 are presented below which are useful for taking care of the saturated control input that introduces nonlinearity in the system dynamics and requires convex approximation for quadratic analysis.

Definition 6 *[182] For a matrix $H(\delta_t) \in \mathbb{R}^{m\times p_2}$ such that $H(\delta_t) = \sum_{i=1}^{2} \sigma_i H_i$, $\sum_{i=1}^{2} \sigma_i = 1$, $0 \leq \sigma_i \leq 1$, $H_i x(t)$ is said to be unsaturated if the following condition is satisfied*

$$|h_j^i x(t)| \leq \bar{u}_j, \ \forall j = 1, \cdots, m, \ i = 1,2, \tag{4.26}$$

where h_j^i represents the j^{th} row of H_i. A set defined as

$$\mathcal{L}(H_i, u_j) := \left\{x(t) \in \mathbb{R}^p : |h_j^i x(t)| \leq \bar{u}_j, \forall j = 1, \cdots, m\right\} \tag{4.27}$$

represents the region in which the control input is unsaturated.

From Definition 4 and (4.26)*, the compact ellipsoid lies inside* $\mathcal{L}(H(\delta_t), u_j)$*, i.e.,* $\bar{\Omega}(P,1) \subset \cap_{i=1}^{2}\mathcal{L}(H_i, u_j)$*, which implies* $\bar{\Omega}(P,1) \subset \mathcal{L}(H(\delta_t), u_j)$*, if* $1 \geq x^T(t)Px(t) \geq \frac{x^T(t)h_j^{i\,T}h_j^i x(t)}{\bar{u}_j^2}$*,* $\forall j, i$*. It can be shown following [182] that it is equivalent to*

$$h_j^i P^{-1} h_j^{i\,T} \leq \bar{u}_j^2,\ j = 1, \cdots, m,\ i = 1, 2. \tag{4.28}$$

Let Γ be a set of $m \times m$ diagonal matrices with diagonal entries taking only binary values of 1 or 0. It is easy to see the cardinality of Γ is 2^m. Let each element of Γ be labeled as $\Gamma_k,\ k = 1, \cdots, 2^m$. Denote $\bar{\Gamma}_k = I - \Gamma_k$. Clearly, $\bar{\Gamma}_k \in \Gamma$. It can be shown following [182] that the saturated control input can be expressed as a convex function presented in the following Lemma.

Lemma 4.5 *[182] For the matrices* $K(\delta_t), H(\delta_t)$ *and* $x(t)$*, if* $x(t) \in \mathcal{L}(H(\delta_t), u_j)$*, then* $\forall\ k = 1, \cdots, 2^m$*, we have*

$$sat\{K(\delta_t)x(t)\} \in Co\left\{\left(\Gamma_k K(\delta_t)x(t) + \bar{\Gamma}_k H(\delta_t)x(t)\right)\right\} \tag{4.29}$$

Using Lemma 4.5, sat$\{u(t)\}$ can be further expressed as

$$\text{sat}\left\{K(\delta_t)x(t)\right\} = \sum_{k=1}^{2^m} \kappa_k \left(\Gamma_k K(\delta_t) + \bar{\Gamma}_k H(\delta_t)\right) x(t) \tag{4.30}$$

where $0 \leq \kappa_k \leq 1$ and $\sum_{k=1}^{2^m} \kappa_k = 1$. The feedback controller for system (4.22) is:

$$u(t) = K(\delta_t)\tilde{x}(t), \tag{4.31}$$

where $K(\delta_t)$ is the controller gain. Now, the overall closed-loop system is given as

$$\begin{bmatrix} \dot{\tilde{x}}(t) \\ z(t) \end{bmatrix} = \begin{bmatrix} \bar{A}_{cl}(\delta_t) & \bar{B}_{cl} \\ \bar{C}_{cl} & 0 \end{bmatrix} \begin{bmatrix} \tilde{x}(t) \\ w(t) \end{bmatrix}, \tag{4.32}$$

where $\bar{A}_{cl}(\delta_t) = \bar{A}(\delta_t) + \bar{B}\bar{K}(\delta_t),\ \bar{B}_{cl} = \bar{B}_w,\ \bar{C}_{cl} = \bar{C}_z$ and $\bar{K}(\delta_t) = \sum_{k=1}^{2^m} \kappa_k \left(\Gamma_k K(\delta_t) + \bar{\Gamma}_k H(\delta_t)\right)$ are the closed-loop matrices.

The main result of this note is now presented in the theorem below.

Theorem 4.6 *The closed-loop TRMS system (4.22) is stable with the controller (4.31) and* $\mathcal{L}_2$ *performance of* γ *is ensured if, for scalars* $\gamma > 0$*,* λ*, there exist* $X = X^T > 0$*,* Z_i*,* Q_i *and* $\Lambda > 0$ *satisfying the below LMI optimization problem:*

$$\textit{Minimize } \lambda^{-2} + \gamma^2$$

subject to

$$\begin{bmatrix} Sym\{\bar{A}_i X + \bar{B}\Gamma_k Z_i + \bar{B}\bar{\Gamma}_k Q_i\} & * & * \\ \bar{B}_w^T & -\gamma^2 I & * \\ \bar{C}_z X & 0 & -I \end{bmatrix} < 0,$$

$$k = 1, 2, 3, 4,\ i = 1, 2 \tag{4.33}$$

$$\begin{bmatrix} -\lambda^{-2}\Lambda & I \\ I & -X \end{bmatrix} \leq 0, \tag{4.34}$$

$$\begin{bmatrix} \bar{u}_j^2 & * \\ q_j^{iT} & X \end{bmatrix} \geq 0,\ j = 1, 2,\ i = 1, 2 \tag{4.35}$$

where q_j^i represents the j^{th} row of Q_i and Λ is a positive definite matrix. λ denotes the estimate of region of attraction. The corresponding controller gain is given as $K_i = Z_i X^{-1}$.

Proof 1 *Consider the qLPV system* (4.22) *with the control input* (4.31)*. Using Lemma 4.3, substituting the closed-loop system matrix as $\bar{A}_{cl}(\delta_t)$ from* (4.32) *and finally taking $K_i X = Z_i$ and $H_i X = Q_i$, one can obtain the LMI condition* (4.33)*.*

Next, for obtaining LMI condition (4.34) *to get a least conservative region of attraction, let $\mathcal{S} := \{x \in \mathbb{R}^n : x^T \Lambda x \leq 1\}$ be a bounded convex ellipsoid containing the equilibrium point. With an aim to find out the maximal region inside $\bar{\Omega}(P, 1)$ with respect to the convex set $\mathcal{S}$, define*

$$\lambda_\Lambda(\bar{\Omega}(P, 1)) := sup\{\lambda > 0|\ \lambda\mathcal{S} \subset \bar{\Omega}(P, 1)\}. \tag{4.36}$$

In other words, our goal is to find the maximal ellipsoid $\lambda_\Lambda(\bar{\Omega}(P, 1))$, satisfying Theorem 1. λ is maximized such that $\lambda\mathcal{S} \subset \bar{\Omega}(P, 1)$. It is equivalent to

$$\frac{\Lambda}{\lambda^2} \geq P. \tag{4.37}$$

Using schur complement, with $X = P^{-1}$, one obtains the LMI condition (4.34). Next, the ellipsoid $(\bar{\Omega}(P, 1))$ is inside $\mathcal{L}(H(\delta_t), u_j)$, i.e., $\bar{\Omega}(P, 1) \subset \mathcal{L}(H(\delta_t), u_j)$, if and only if condition (4.28) holds. Again applying schur complement to (4.28)*, one obtains LMI* (4.35)*.*

4.1.3.5 Regional pole-placement

This section considers placing the eigenvalues of the closed-loop system in a desired LMI region [12, 145, 183] using state feedback control with a view to improving the transient performance for known damping ratio and decay rate. This becomes necessary since the $\mathcal{L}_2$ based control in the previous section lacks in ensuring one although it yields a good robust performance. Now, following [12], we give the below Theorem for use in controller design.

Theorem 4.7 *The closed-loop eigenvalues of system (4.32) are placed in the LMI region $\mathcal{D}_C(\alpha, \theta)$ if, for a scalar α, there exist matrices $X = X^T > 0$, Q_i and Z_i such that the LMI given below is feasible.*

$$\begin{bmatrix} \sin\theta Sym\{\bar{\Phi} + \alpha X\} & * \\ \cos\theta(\bar{\Phi}^T - \bar{\Phi}) & \sin\theta Sym\{\bar{\Phi} + \alpha X\} \end{bmatrix} < 0 \tag{4.38}$$

where $\bar{\Phi} = \bar{A}_i X + \bar{B}\Gamma_k Z_i + \bar{B}\bar{\Gamma}_k Q_i$. $\mathcal{D}_C(\alpha, \theta)$, as shown in Fig. 1.5, denotes an LMI region corresponding to a minimum decay rate (α) and a minimum damping (ζ).

Proof 2 *Consider the following LMI, first, for a conic sector with center at origin and inner angle 2θ.*

$$\begin{bmatrix} \sin\theta(\bar{A}_{cl}(\delta_t)X + X\bar{A}_{cl}(\delta_t)^T) & * \\ \cos\theta(X\bar{A}_{cl}(\delta_t)^T - \bar{A}_{cl}(\delta_t)X) & \sin\theta(\bar{A}_{cl}(\delta_t)X + X\bar{A}_{cl}(\delta_t)^T) \end{bmatrix} < 0. \tag{4.39}$$

Now for the i^{th} polytope vertex, $\bar{A}_{cl_i} = \bar{A}_i + \bar{B}(\Gamma_k K_i + \bar{\Gamma}_k H_i)$. Then substituting the value of K_i from Lemma 4.5, we have $\bar{A}_{cl_i}X = \bar{A}_i X + \bar{B}\Gamma_k Z_i + B\bar{\Gamma}_k Q_i)$, with $Z_i = K_i X$ and $Q_i = H_i X$. Using this value of $\bar{A}_{cl_i}X$ in (4.39), we get

$$\begin{bmatrix} \sin\theta Sym\{\bar{\Phi}\} & * \\ \cos\theta(\bar{\Phi}^T - \bar{\Phi}) & \sin\theta Sym\{\bar{\Phi}\} \end{bmatrix} < 0. \tag{4.40}$$

Next, the LMI condition for a subset of half-plane with decay rate α is given as

$$\bar{A}_{cl}(\delta_t)X + X\bar{A}_{cl}(\delta_t)^T + 2\alpha X < 0. \tag{4.41}$$

Now, using similar steps as above, (4.41) can be rewritten for the i^{th} vertex as

$$Sym\{\bar{A}_i X + \bar{B}\Gamma_k Z_i + B\bar{\Gamma}_k Q_i)\} + 2\alpha X < 0. \tag{4.42}$$

Finally, combining (4.40) and (4.42), we get (4.38).

Note that to obtain the global minimum γ, the set of LMIs has been solved using the LMI Toolbox in MATLAB [158]. To enhance the disturbance rejection capability, a tradeoff needs to be struck between minimizing attenuation level γ and enlarging the domain of attraction by maximizing λ^2. In order to balance between them, maximizing λ^2 is equivalent to minimizing λ^{-2} and hence, the problem can be combined into a single one by minimizing the term $\lambda^{-2} + \gamma^2$.

The following problem is solved for controller design for the TRMS.

Problem 2 *Given the knowledge of user-specified parameters $\theta,\ \alpha, \Gamma_k$ and Λ, design a robust PI controller with $\mathcal{L}_2$ performance γ, under actuator saturation subject to LMI conditions* (4.33)*, (4.34),* (4.35) *and* (4.38) *to provide the desired set point tracking such that $\lambda^{-2} + \gamma^2$ is minimized. The following Algorithm 1 summaries the procedure.*

Algorithm 1

Given: *$\theta,\ \alpha,\ \Gamma_k$ and Λ.*

Step 1*: Solve Problem 1 by solving LMI conditions (20), (21), (22) and (25).*

Step 2*: Calculate $Z_i,\ Q_i, K_i\ \lambda,\ \gamma$ and X.*

Step 3*: Calculate $\sigma(\delta_t)$ using (13) and subsequently $K(\delta_t)$ using Remark 3.*

4.1.3.6 Experimental results

The proposed design is implemented on a 2-DOF helicopter system and the results are presented in this section. The experimental setup of a Quanser make 2-DOF helicopter [150] is shown in Fig. 4.10. For implementation of the proposed design technique on 2-DOF helicopter model, we have considered the variation in the pitch angle as $x_1 \in [-35^\circ, -5^\circ]$ and maximum value that the state x_4 can take is assumed to be 3 deg/sec. Thus, the overall uncertain parameter δ_t lies between -1.41 and -0.26. Also, since the number of inputs is 2, the cardinality of Γ is 4 as stated in the paragraph following (4.28), hence $\Gamma_1 = \begin{bmatrix} 0 & 0 \\ 0 & 0 \end{bmatrix}$, $\Gamma_2 = \begin{bmatrix} 1 & 0 \\ 0 & 0 \end{bmatrix}$, $\Gamma_3 = \begin{bmatrix} 0 & 0 \\ 0 & 1 \end{bmatrix}$, $\Gamma_4 = \begin{bmatrix} 1 & 0 \\ 0 & 1 \end{bmatrix}$. Now, using above values, the

Table 4.7: Control gains for different controllers

Controller	Feedback gains
Optimal LQR-I [150]	$K = \begin{bmatrix} 18.9 & 1.98 & 7.49 & 1.53 & 7.03 & 0.77 \\ -2.22 & 19.4 & -0.45 & 11.9 & -0.77 & 7.03 \end{bmatrix}$
LQR-I (APSO) [172]	$K = \begin{bmatrix} 19.24 & 2.17 & 9.17 & 1.27 & 10.37 & 1.39 \\ -1.79 & 14.29 & -0.31 & 6.21 & -0.83 & 7.63 \end{bmatrix}$
qLPV Robust PI Centralised	$K_1 = \begin{bmatrix} 14.08 & 0.84 & 4.64 & 0.25 & 2.42 & 0.16 \\ 1.58 & 45.18 & 2.63 & 21.12 & 0.31 & 7.89 \end{bmatrix}$ $K_2 = \begin{bmatrix} 13.91 & 1.71 & 4.62 & 1.00 & 2.39 & 0.32 \\ 3.80 & 45.10 & 1.79 & 20.99 & 0.71 & 7.88 \end{bmatrix}$
qLPV Robust PI Decentralised	$K_1 = \begin{bmatrix} 15.07 & 0 & 6.69 & 0 & 1.78 & 0 \\ 0 & 54.65 & 0 & 36.73 & 0 & 6.50 \end{bmatrix}$ $K_2 = \begin{bmatrix} 15.34 & 0 & 6.67 & 0 & 1.81 & 0 \\ 0 & 54.00 & 0 & 36.22 & 0 & 6.43 \end{bmatrix}$

system matrices of model (4.22) in polytopic form are given as:

$$A_1 = \begin{bmatrix} 0 & 0 & 1 & 0 \\ 0 & 0 & 0 & 1 \\ 0 & 0 & -9.5935 & 0.7605 \\ 0 & 0 & -1.5209 & -3.6067 \end{bmatrix}, B = \begin{bmatrix} 0 & 0 \\ 0 & 0 \\ 2.4463 & 0.0815 \\ 0.2484 & 0.8166 \end{bmatrix}, A_2 = \begin{bmatrix} 0 & 0 & 1 & 0 \\ 0 & 0 & 0 & 1 \\ 0 & 0 & -9.5935 & 0.1402 \\ 0 & 0 & -0.2805 & -3.6067 \end{bmatrix},$$

$$B_w = \begin{bmatrix} 0 & 0 & 0.7440 & 0 \end{bmatrix}^T, C_z = I_{4\times 4},\ \delta_t \in [-1.41, -0.26]$$

The parameters used for PI controller design for solving the optimization Problem 2 are $\alpha = 0.1$, $\theta = 70^\circ$ and $\Lambda = I_6$. Solving Problem 1, we get $\gamma = 0.05$ and $\lambda = 0.92$. The same are used for implementation on the real-time model by solving the LMIs and the controller gains are provided in Table 4.9. The saturation limits for the input to pitch motor is ± 24 volts (i.e., $\bar{u}_1 = 24$) and that to the yaw motor is ± 15 volts (i.e., $\bar{u}_2 = 15$). Also, note that K_1 and K_2 provided in the table for robust controllers correspond to initial values of the gains. Overall gains can be computed using Remark 4.4.

A comparative study is carried out for a square input with peak to peak amplitude of 4° and the various state and control input responses are shown. The existing criteria used for comparison are the techniques of Optimal LQR-Integral [150] and Adaptive

Table 4.8: Error Performance for Different Controllers

Controllers	IAE		ISE	
	Pitch	Yaw	Pitch	Yaw
Optimal LQR-I [150]	14.97	81.29	9.6	173.24
LQR-I (APSO) [172]	20.70	131.50	12.60	409.05
qLPV Robust PI Centralized	22.17	47.28	13.91	89.91

Particle Swarm Optimization (APSO) [172]. The pitch and yaw responses for the various controllers are provided in Fig. 4.19 and Fig. 4.20, respectively. An error analysis for a numerical comparison of the obtained responses is given based on IAE and ISE indices in Table 4.8. It can be observed that the robust controller performs well with a good transient response, without significant oscillations in the pitch response with improved steady state response for yaw angle tracking. Next, a decentralized qLPV controller

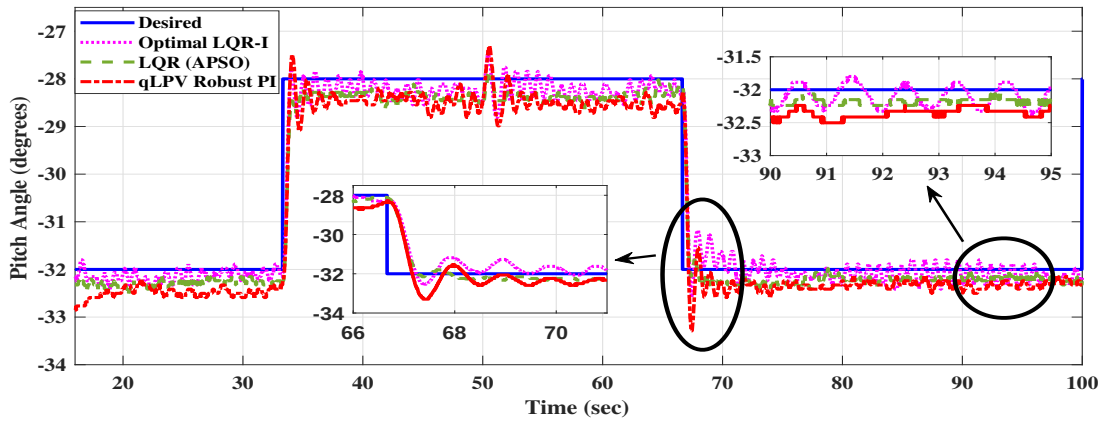

Figure 4.19: Evolution of pitch angle with time

is designed and compared with its counterpart designed above. The experimental yaw and pitch responses are shown in Figs. 4.21 and 4.22, along with their respective control inputs in Figs. in 4.23 and 4.24. To verify Remark 4, a sine wave of 0.1 Hz frequency and peak-peak amplitude of 4° was used as a reference for comparison instead of a step input. This is because a step response could have only a small effect of coupled dynamics to show the performance of decentralized method against cross-interactions between the pitch and yaw responses. Hence, the tracking result was verified by using a time varying trajectory− a sinusoidal function in our case. As is stated in the remark, it is observed

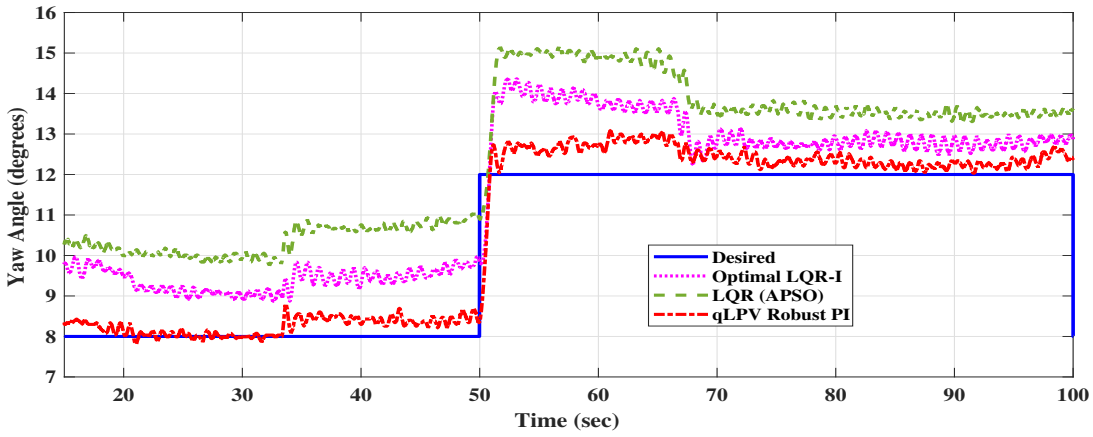

Figure 4.20: Evolution of yaw angle with time

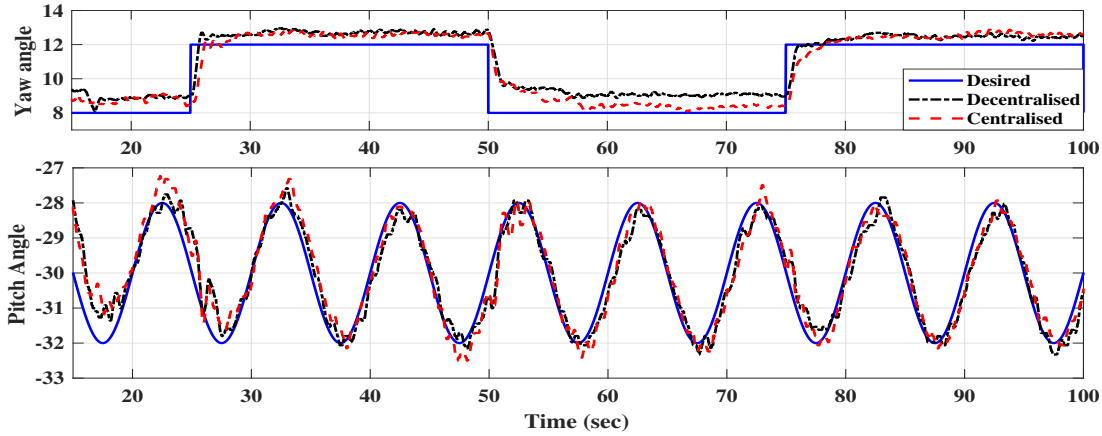

Figure 4.21: Comparison of evolution of pitch and yaw angle for centralized and decentralized robust PI controller

from both the Figs. 4.21 and 4.22 that the response in one state (pitch angle in Fig. 4.21 and yaw angle in Fig. 4.22) for step change in the other (yaw angle in Fig. 4.22 and pitch angle in 4.21) is less aggressive due to additional couplings being prevented by the decentralized controller, hence giving a good tracking performance under the adaptive scheduling of the gains. At other instances the decentralized controller gives nearly good performance as the centralized one.

Figures 4.23 and 4.24 show a comparison between the control inputs for pitch and yaw angles for the centralized and decentralized cases. From the figures, it can be observed that the transients for both the states are less aggressive for the decentralized case, thus reducing the amount of control effort required for efficient tracking. Next, Figure 4.25 shows an estimate of the region of attraction (ROA) under (4.36), using the Lya-

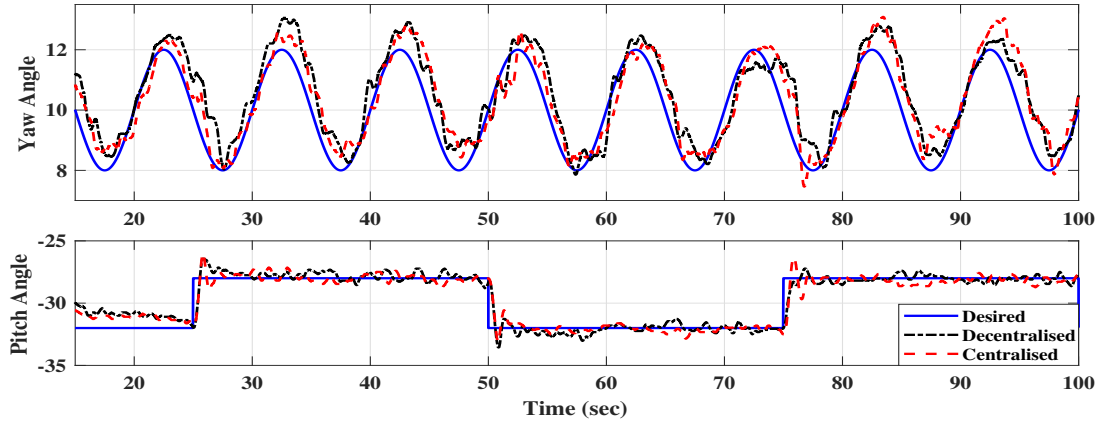

Figure 4.22: Comparison of evolution of yaw and pitch angle for centralised and decentralised robust PI controller

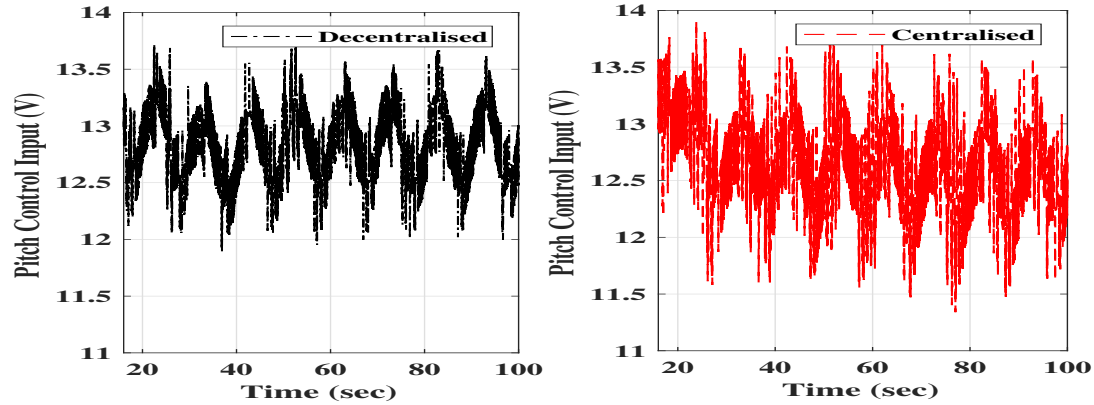

Figure 4.23: Time evolution of control input for pitch angle

punov matrix $P = \begin{bmatrix} 3.1621 & 0 & 0.5964 & 0 & 0.1321 & 0 \\ 0 & 2.9562 & 0 & 0.5436 & 0 & 0.1231 \\ 0.5964 & 0 & 0.2855 & 0 & 0.0256 & 0 \\ 0 & 0.5436 & 0 & 0.2688 & 0 & 0.0233 \\ 0.1321 & 0 & 0.0256 & 0 & 0.0355 & 0 \\ 0 & 0.1231 & 0 & 0.0233 & 0 & 0.0351 \end{bmatrix}$. Since the region of attraction (ROA) for the closed-loop system (4.22) is a hypersphere in six dimensions, we give a 2-dimensional ROA corresponding to position ($\tilde{x}_1$, $\tilde{x}_2$) states. To obtain such an ROA, the other states (velocity and integral states) are assumed to be zero. The following Figure 4.25 shows the ROA corresponding to position states. Other ROAs for the velocity and integral states can be obtained in a similar way. It is to be further noted that if we

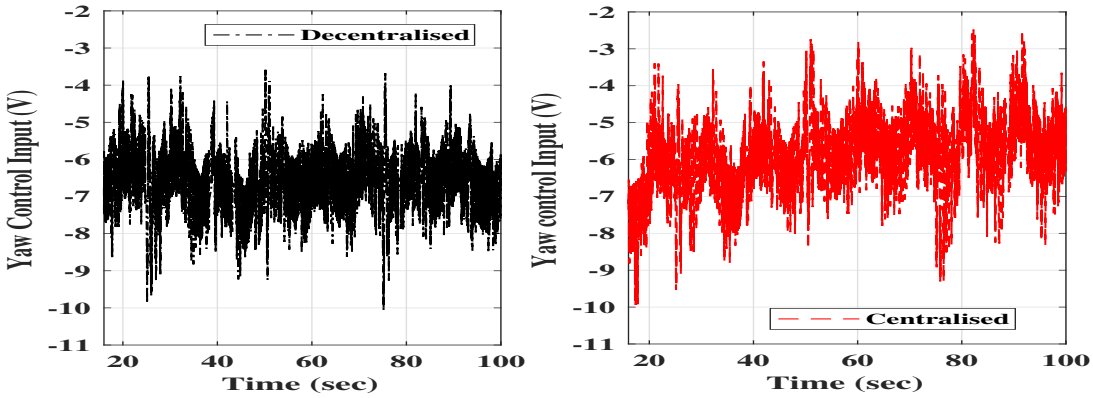

Figure 4.24: Time evolution of control input for yaw angle

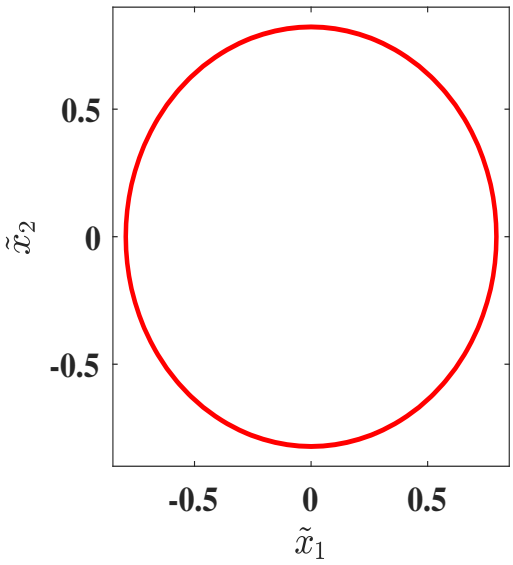

Figure 4.25: Region of Attraction (involving states $\tilde{x}_1,\ \tilde{x}_2$)

consider all the states at once, the combined ROA will differ from the one shown here.

Finally, to show the advantage of incorporating LMIs corresponding to saturation constraints in our design, experimental results without taking these constraints into the design problem is compared with Problem 2 results. The corresponding pitch and yaw angle responses are shown in Fig. 4.26. Also, a comparison of the control input, with and without saturation constraints is shown in Fig. 4.27. The effect of saturation can be easily seen in that the pitch and yaw angles do not show set point tracking and the control input is highly oscillatory and saturates during the operation due to high control gains. It is to be further noted that the control input in some of the figures does not involve chattering, rather these are low-frequency oscillations as it appears in the figures.

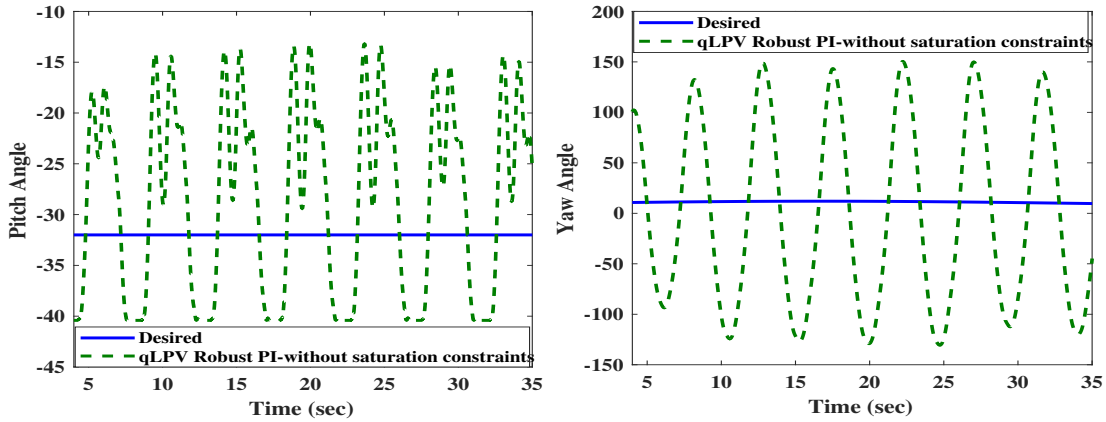

Figure 4.26: Time evolution of pitch and yaw angle without considering saturation constraints

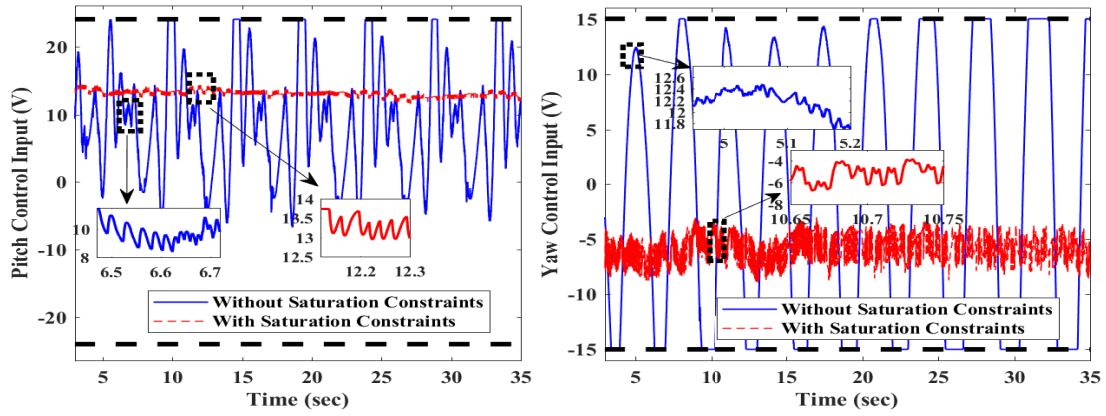

Figure 4.27: Comparison of control input with and without considering saturation constraints (Bold black margins denote saturation limits)

It appears so because of the time cramped visual of oscillation. This is clearly visible from the zoomed sub-figure within Figure 4.27.

4.1.4 SOF controller design for TRMS

This section considers the Quanser 2-DOF helicopter experimental setup [150] to demonstrate the design method presented in Problem 1 in chapter 2, i.e., designing the SOF controller for the polytopic systems subject to actuator saturation. The helicopter system is actuated by two DC motors [184], one for the pitch and other for the yaw plane. The setup is shown in Fig. 4.10 and the corresponding parameters are taken from Table 4.4.

The same nonlinear dynamic model of the helicopter system (4.13), presented in pre-

vious section is considered for the design. In the previous design case, we have considered the state feedback controller design but in this section, SOF controller in the presence of actuator saturation is considered for the tracking control of 2-DOF helicopter model. The polytopic representation of nonlinear dynamics of 2-DOF helicopter model (4.13) is expressed as:

$$\dot{x}(t) = \bar{A}(\theta)x(t) + \bar{B}sat\{u(t)\} + \bar{B}_w w(t)$$
$$\bar{z}(t) = \bar{C}_z x(t), \bar{y}(t) = \bar{C}x(t), u(t) = \begin{bmatrix} V_1(t) & V_2(t) \end{bmatrix}^T,$$

where $\theta = x_4(t)sin(x_1(t))cos(x_1(t))$ is the uncertain parameter and $w(t) = cos(x_1(t))$. It is considered that the pitch angle varies as $x_1(t) \in [-35^\circ, \ -25^\circ]$ and the yaw velocity $x_4(t) \in [-3, 3]$ so that the uncertain parameter $\theta \in [-1.41, -1.15]$. Thus, $\bar{A}(\theta) = \theta A_1 + (1-\theta)A_2 \in Co\{A_1, A_2\}$, with

$$\bar{A}_1 = \begin{bmatrix} 0 & 0 & 1 & 0 \\ 0 & 0 & 0 & 1 \\ 0 & 0 & -9.5935 & 0.7605 \\ 0 & 0 & -1.5209 & -3.6067 \end{bmatrix}, \bar{A}_2 = \begin{bmatrix} 0 & 0 & 1 & 0 \\ 0 & 0 & 0 & 1 \\ 0 & 0 & -9.9539 & 0.6197 \\ 0 & 0 & -1.2394 & -3.6067 \end{bmatrix}, \bar{B}_w = \begin{bmatrix} 0 \\ 0 \\ 0.7440 \\ 0 \end{bmatrix},$$
$$\bar{B} = \begin{bmatrix} 0 & 0 \\ 0 & 0 \\ 2.4463 & 0.0815 \\ 0.2484 & 0.8166 \end{bmatrix}, \ \bar{C}_z = 10^{-2} \times I_{4\times 4}, \ \bar{C} = \begin{bmatrix} 1 & 0 & 0 & 0 \\ 0 & 1 & 0 & 0 \end{bmatrix}.$$

Consider a PI controller to be designed as $u(t) = K_p\bar{C}x(t) + K_I\int_0^t \bar{y}(\tau)d\tau$. $K_p \in \mathbb{R}^{2\times 2}, K_I \in \mathbb{R}^{2\times 2}$ are the gain matrices of the PI controller. For this, the augmented system states are $r(t) = \begin{bmatrix} x^T(t) & \int_0^t \bar{y}^T(\tau)d\tau \end{bmatrix}^T$ with its dynamics as

$$\dot{r}(t) = A(\theta)r(t) + Bsat\{u(t)\} + B_w w(t),$$
$$z(t) = C_z r(t), \ y(t) = Cr(t), \tag{4.43}$$

where $A(\theta)$, B, C, B_w and C_z represent the augmented system matrices, given by $A(\theta) = \begin{bmatrix} \bar{A}(\theta) & 0 \\ \bar{C} & 0 \end{bmatrix}$, $B = \begin{bmatrix} \bar{B} \\ 0 \end{bmatrix}$, $C = \begin{bmatrix} \bar{C} & 0 \\ 0 & I \end{bmatrix}$, $B_w = \begin{bmatrix} \bar{B}_w \\ 0 \end{bmatrix}$, $C_z = \begin{bmatrix} \bar{C}_z & 0 \end{bmatrix}$ and $y(t)$ is the measured output of the augmented system. For system (4.43), the feedback controller is $u(t) = Ky(t)$, where $K = \begin{bmatrix} K_p & K_I \end{bmatrix}$ denotes the controller gain.

The saturation limits for the input to pitch motor is ±24 volts (i.e., $\bar{u}_1 = 24$) and that to the yaw motor is ±15 volts (i.e., $\bar{u}_2 = 15$). Further, $Q = \begin{bmatrix} 0 & 0 \\ 0 & 0 \\ -1 & 0 \\ 0 & -1 \\ 0 & 0 \\ 0 & 0 \end{bmatrix}$ and $R = \begin{bmatrix} 1 & 0 & 0 & 0 \\ 0 & 1 & 0 & 0 \\ 0 & 0 & 0 & 0 \\ 0 & 0 & 0 & 0 \\ 0 & 0 & 1 & 0 \\ 0 & 0 & 0 & 1 \end{bmatrix}$. The controller gain K is designed by solving the LMI in Problem 1 with parameters $\lambda = 1.054$, $\bar{\alpha} = 8.0040$, $\gamma = 0.01$ and $\bar{\rho} = 0.9408$. The same is implemented in real-time on the 2-DOF helicopter system.

Figures 4.28 and 4.29 demonstrate experimental results on the pitch and yaw tracking performances under the proposed design and two existing state feedback techniques, namely Optimal LQR-I [150] and LQR (APSO) [172]. Additionally, to show the advantage of incorporating LMIs corresponding to saturation constraints in our design, experimental result of the control input, without taking these constraints into the design problem is compared with the case where they are included in the design problem. This comparison is shown in Fig. 4.30 and the corresponding gain matrix is

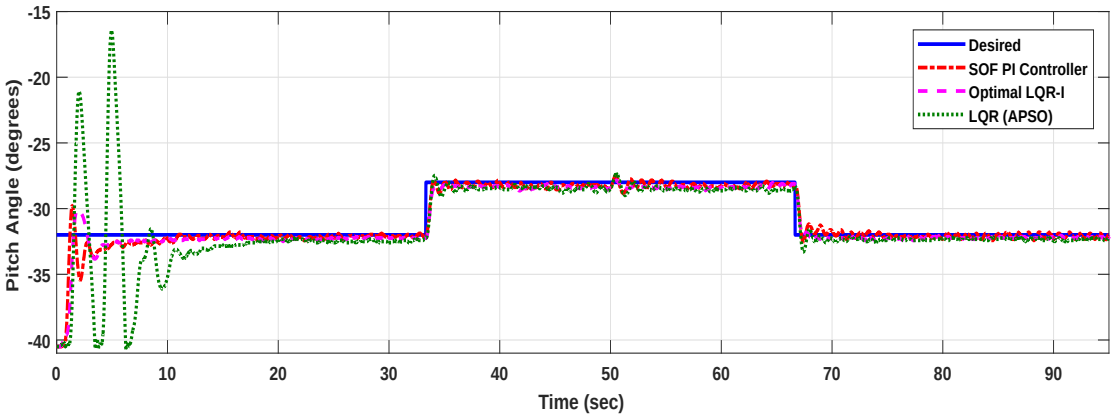

Figure 4.28: Experimental result: Pitch angle variation of the 2-DOF helicopter

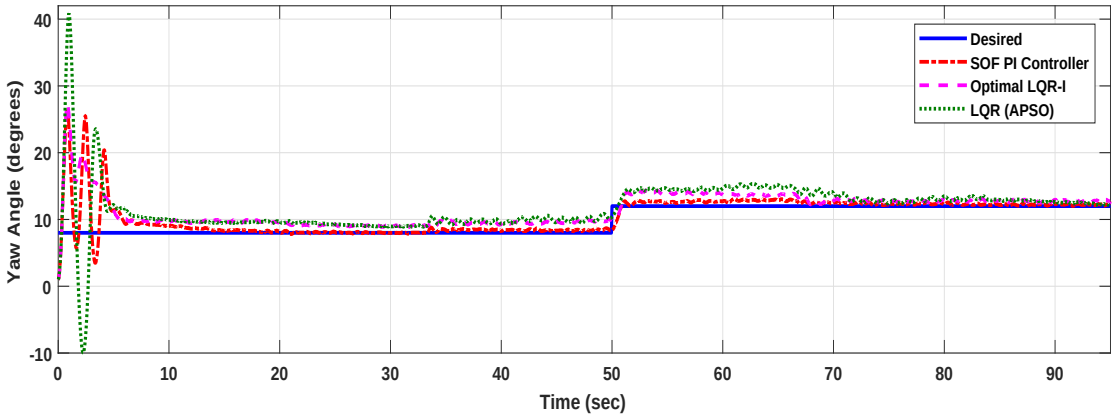

Figure 4.29: Experimental result: Yaw angle variation of the 2-DOF helicopter

$K = \begin{bmatrix} 31.4386 & -13.7787 & -3.1591 & 3.6306 \\ 9.5819 & -68.1250 & 12.5885 & -19.7414 \end{bmatrix}$. The effect of saturation can be easily seen in that the control input is highly oscillatory and saturates during the operation due to high control gains. The controller gain values and the error performance in terms

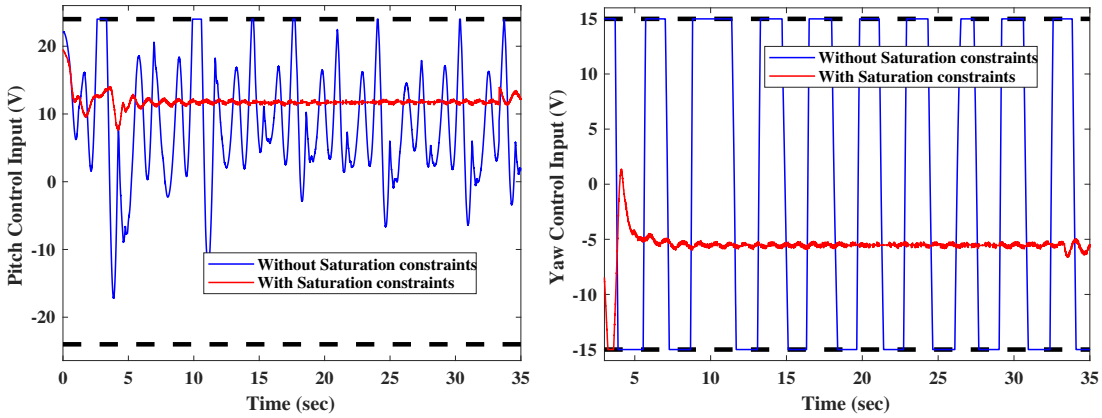

Figure 4.30: Experimental result: Comparison of control input of 2-DOF helicopter with and without considering saturation constraints (Bold black margins denote saturation limits)

of Integral Square Error (ISE) and Integral Absolute Error (IAE), are computed and provided in tables 4.9 and 4.10, respectively.

It can be seen that the proposed output feedback design gives similar performance both in the transient and steady state conditions, when compared to the state feedback designs. Further, the control inputs are well in the saturation limits and the step demands in the angular positions are achieved satisfactorily, though the initial transient during

Table 4.9: Controller gains and error performance for different controllers

Controller	Controller gain $K = [K_p\ K_I]$
SOF PI controller (Theorem 2)	$\begin{bmatrix} 5.3944 & 0.1506 & 0.6814 & 0.0229 \\ -1.4428 & 8.3145 & -0.1707 & 0.9897 \end{bmatrix}$
LQR-I [150]	$\begin{bmatrix} 18.9 & 1.98 & 7.49 & 1.53 & 7.03 & 0.77 \\ -2.22 & 19.4 & -0.45 & 11.9 & -0.77 & 7.03 \end{bmatrix}$
LQR-I (APSO) [172]	$\begin{bmatrix} 19.24 & 2.17 & 9.17 & 1.27 & 10.37 & 1.39 \\ -1.79 & 14.29 & -0.31 & 6.21 & -0.83 & 7.63 \end{bmatrix}$

Table 4.10: Controller gains and error performance for different controllers

Controller	IAE		ISE	
	Pitch	Yaw	Pitch	Yaw
SOF PI controller (Theorem 2)	14.97	44.09	9.6	44.12
LQR-I [150]	14.97	81.29	9.6	173.24
LQR-I (APSO) [172]	20.70	131.50	12.60	409.05

starting is a bit more due to arbitrary initial positioning. It may be noted that most of the existing designs of the helicopter model [172,184] attempt to obtain reduced controller gain by imposing constraints on the gain parameters to avoid saturation. Neither output feedback nor saturation based design even for state feedback has been attempted so far.

From the experimental results, we can conclude that the SOF controller is successfully designed and implemented on the real-time 2-DOF helicopter setup and the desired setpoint tracking of both the pitch and yaw angles is achieved.

4.2 Discrete-time design

4.2.1 Boost Converter

In the previous chapter 3, a new approach for convex approximation of constant damping ratio has been proposed for DT systems which is an unsolved problem in literature. The non-convex damping region is approximated to an elliptical segment that represents an LMI region. Pole-placement in such LMI region through design of different control

strategy has been carried out. The motive behind this is to enhance the transient behavior of the closed-loop systems. Numerical examples are provided there to show the effectiveness of the proposed design. Further, its application is demonstrated for a boost converter. Simulation results are provided to show how the proposed control strategy can be employed to enhance its transient responses when subjected to input voltage and load variations.

A similar performance based design has been carried out in [34] but for (i) state feedback control, which is often complex to implement, and (ii) with a polytopic approximation of the damping region. An explicit comparison with such polytopic region is not carried out since such approximation accuracy depends on number of vertices considered, which increases computational burden considerably with increase in number of vertices (or the accuracy) that enables a trade-off between computational complexity in terms of the number of LMIs and the betterment of the approximation. The present design does not involve this drawback and is also superior in the aspect that not only the state feedback controller but also output feedback controllers of different types, such as static, dynamic, PI can be designed as demonstrated subsequently.

The boost regulator circuit is shown in Fig. 4.31. The CT linearized dynamics of

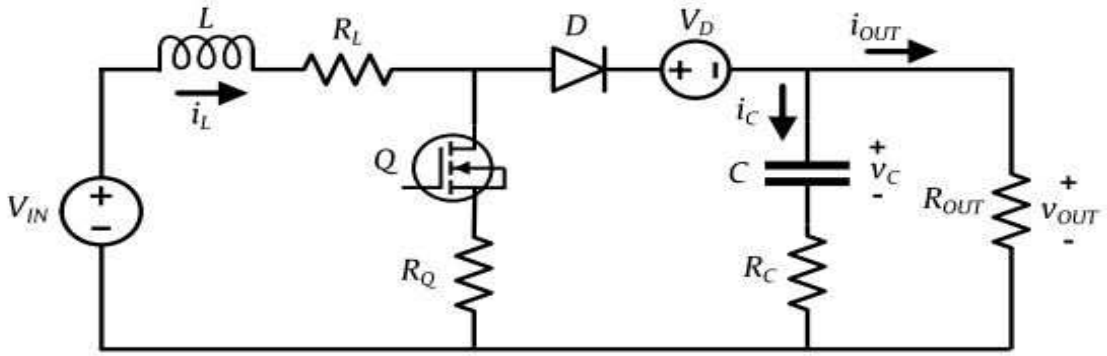

Figure 4.31: Boost step-up converter circuit diagram

boost converter is given as [34]:

$$\begin{aligned} \dot{x}_{con}(t) &= A_{con}x_{con}(t) + B_{con}u(t), \\ y_{con}(t) &= C_{con}x_{con}(t), \end{aligned} \tag{4.44}$$

with

$$A_{con} = \begin{bmatrix} -\frac{R_{OUT}R_C+\sigma(\delta^{eq}R_Q+R_L)}{\sigma L} & -\frac{\bar{\delta}(R_{OUT}-2R_C)}{\sigma L} \\ \frac{R_{OUT}}{\sigma C} & -\frac{1}{\sigma C} \end{bmatrix},$$

$$B_{con} = \begin{bmatrix} \frac{(V_I-\bar{\delta}V_D)(R_{OUT}(\sigma\bar{\delta}+R_C\delta^{eq})-\sigma R_Q)+\beta V_D}{\beta L} \\ -\frac{(V_{IN}-\bar{\delta}V_D)R_{OUT}}{\beta C} \end{bmatrix},$$

$$C_{con} = \begin{bmatrix} \frac{R_C(1-\delta)}{\frac{R_{OUT}+R_C-2R_C\delta}{R_{OUT}}} & \frac{1}{\frac{R_{OUT}+R_C-2R_C\delta}{R_{OUT}}} \end{bmatrix}$$

where $x_{con}(t) = [i_L(t)\ v_C(t)]^T$ is the state vector, V_{OUT} and duty cycle (δ) are the output and input variables, respectively. $\bar{\delta} = (1-\delta^{eq})$, δ^{eq} is the nominal duty cycle, $\sigma = R_{OUT} - R_C$ and $\beta = R_{OUT}(R_{OUT} - 2R_C)\bar{\delta}^2 + R_{OUT}R_C\bar{\delta} + R_Q\sigma\delta^{eq} + R_L\sigma$. The inductor current ($i_L$) and the capacitor voltage (v_C) are the two state variables. The numerical values of the involved parameters [1] are considered as in [34] for constructing a comparison. The control design objective is to govern the transient response in terms of the decay rate (σ) and the damping factor (ζ) in presence of uncertain input voltage V_{IN} and load resistance R_{OUT}.

A $\pm 1.5\%$ variation in the V_{IN} is considered. The R_{OUT} is assumed to be in the range of 44.6 Ω and 73 Ω. The operating condition is considered as $V_{OUT} = 45V$. The corresponding nominal duty cycle (δ^{eq}) is 0.576. The two uncertain parameters V_{IN} and R_{OUT} lead to four polytope vertices with $\bar{N} = 2$. The four vertices of the DT polytopic model are obtained corresponding to these vertices discretized with sampling time of 1 ms. The design specifications considered are $\zeta = 0.5912$ and $\sigma = -0.2$ corresponding to 10 % overshoot and settling time of 25 ms [34].

A state feedback controller is designed using Theorem 3.22 for a comparison with [34]. In addition, a SOF controller is also designed using Theorem 3.23. The corresponding closed-loop poles with the controller gains are tabulated in Table 4.11. It should be noted that the SOF controller comprises of only a control gain parameter compared to two parameters for the state feedback case and still able to allocate the poles in the desired damping region $\hat{\mathcal{D}}_2$. Fig. 4.32 shows the open-loop and closed-loop poles under SOF controller for the four polytope vertices. Further, the simulation results for the state feedback controller of [34] and the designed state and SOF controller responses are shown

[1] $L = 900\mu H$, $C = 680\mu F$, $R_L = 59.7m\Omega$, $R_C = 155.8m\Omega$, $R_Q = 68m\Omega$, $R_{OUT} = 56\Omega$, $V_D = 1.7V$, $V_{IN} = 20V$

Table 4.11: Closed-Loop Poles with Controllers Gains

Controller Gain	Closed-loop poles
State Feedback Controller ([34])	
$K_s = \begin{bmatrix} -0.01707 & 0.00493 \end{bmatrix}$	1) -0.1378, 0.4756 2) -0.1859, 0.4968 3) -0.1238, 0.4514 4) -0.1732, 0.4739
State Feedback Controller (Present)	
$K_s = \begin{bmatrix} -0.0072 & 0.0075 \end{bmatrix}$	1) 0.1702, 0.6695 2) 0.1332, 0.6948 3) 0.1711, 0.6521 4) 0.1334, 0.6779
SOF Controller	
$K_o = 0.0084$	1) 0.3700, 0.8622 2) 0.3407, 0.8917 3) 0.3609, 0.8513 4) 0.3317, 0.8804

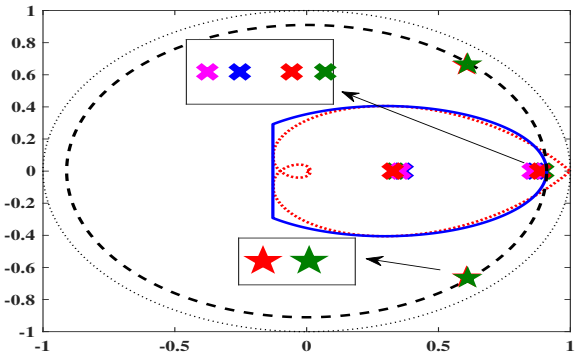

Figure 4.32: Pole map for the boost converter : (i) Open-loop poles (star marked) and (ii) Closed-loop poles for the SOF controller at the four polytope vertices (cross marked)

in Fig. 4.33. The capacitor is initially charged to 35V. The obtained results are simulated considering changes in R_{OUT} as 56Ω for $t \in [0,\ 0.1)$ *sec*, 62Ω for $t \in [0.1,\ 0.15)$ *sec* and 50Ω for $t \geq 0.15$ *sec*. Similarly, V_{IN} is considered to change as $20V$ for $t \in [0,\ 0.2)$ *sec*, $20.3V$ for $t \in [0.2,\ 0.25)$ *sec* and $19.7V$ for $t \geq 0.25$ *sec*. It can be seen that the response in V_{OUT} under the proposed criteria shows a significantly lesser overshoot than the one for [34], coupled with a lesser settling time as well. In addition the response under SOF controller, although designed using less information than the state feedback one, shows a similar response, except for oscillations in the steady state. Finally, the state and output feedback PI controllers design are considered for simulation with the same variations in R_{OUT} and V_{IN} as discussed above. The state feedback PI structure is shown in Fig. 4.34.

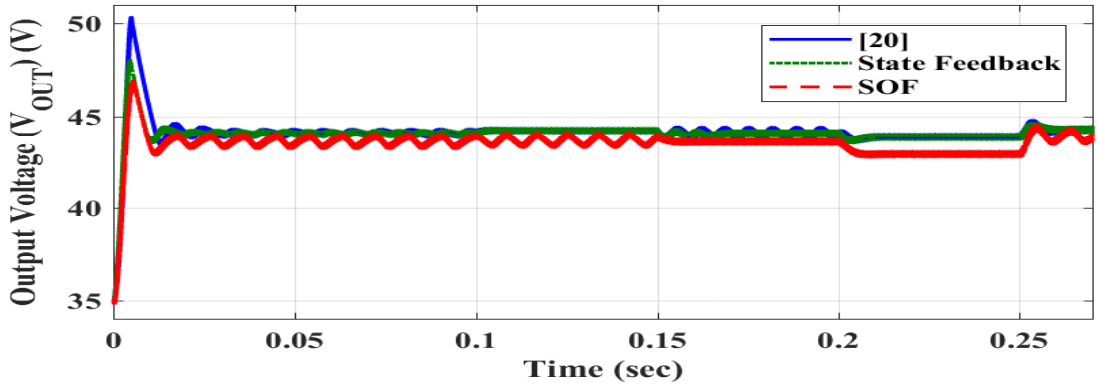

Figure 4.33: Output voltage response for different controllers

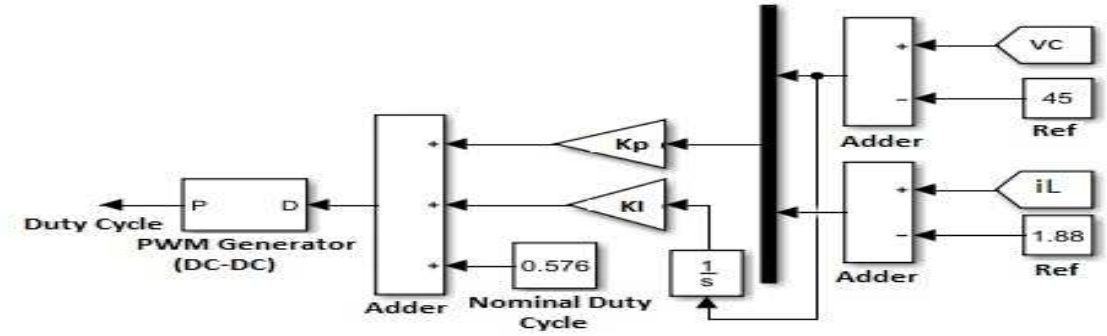

Figure 4.34: State Feedback PI controller structure

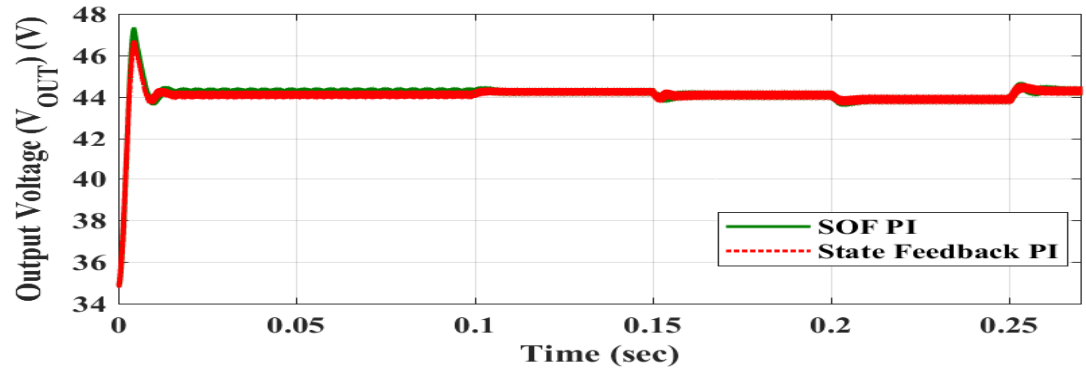

Figure 4.35: Output voltage response of State feedback and SOF PI controllers

For output feedback PI, the controller structure is similar to the one in Fig. 4.34 except that only the available output, i.e., V_{OUT}, is fed back to the controller while the state $i_L(t)$ unavailable. The designed state feedback PI controller gains are $K_p = [-0.0175\ 0.0027]$ and $K_I = -0.0018$ and SOF PI controller gains are $K_p = 0.0047$ and $K_I = -0.0003$. Fig. 4.35 shows the responses of the output voltage under the state and SOF PI controller. It can be again observed that the response under SOF PI controller is similar to the state

feedback controller response apart from a slightly higher overshoot due to the fact that the poles are placed near the region boundary, while meeting the performance specification appropriately.

4.3 Summary

This chapter presents a methodology for designing the robust LMI based PI controller for real–time hardware setups such as a coupled tank system and a 2–DOF helicopter. A new approach for handling nonlinear CT systems in the form of polytopic model has been proposed. The nonlinear system model is represented in a linear form with parametric uncertainties that does not involve neglecting any higher-order term. Additionally, regional pole placement criterion considered in the design improves the closed-loop transient behavior of the CT systems.

Next, a robust qLPV PI controller is designed for tracking control of a TRMS. The system is modeled as a qLPV polytopic one, without any approximation of the higher order terms. This approach, along with adaptable qLPV structure prevents any additional cross-coupling appearing between the dynamics of both the pitch and yaw planes, thereby reducing the cross coupling through the controller gains. The controller gain is kept within practical limit by incorporating actuator saturation criterion.

Moreover, the efficacy and application of the SOF controller design for polytopic systems in the presence of actuator saturation presented in chapter 2 is illustrated through the implementation on hardware setup of 2–DOF helicopter. Experimental results are provided to demonstrate the effectiveness of proposed design method.

Further, an application and effectiveness of the proposed control strategy presented in chapter 3 is demonstrated for a boost converter, even for PI controller design in order to improve the transient behavior of the boost converter subject to variation in input voltage and load resistance. Simulation results are presented to show its effectiveness.

The next chapter summarizes the work of the thesis, and forecasts the possible endeavors in the context of SOF design methods.